1980

# The crystal structure determinations of Lu–b3–sS–b4–s, nonstoichiometric Nb–b1–s–ḅ06–sS–b2–s, and three Group VIII coordination complexes

Douglas Ray Powell
*Iowa State University*

## INFORMATION TO USERS

This was produced from a copy of a document sent to us for microfilming. While the most advanced technological means to photograph and reproduce this document have been used, the quality is heavily dependent upon the quality of the material submitted.

The following explanation of techniques is provided to help you understand markings or notations which may appear on this reproduction.

1. The sign or "target" for pages apparently lacking from the document photographed is "Missing Page(s)". If it was possible to obtain the missing page(s) or section, they are spliced into the film along with adjacent pages. This may have necessitated cutting through an image and duplicating adjacent pages to assure you of complete continuity.

2. When an image on the film is obliterated with a round black mark it is an indication that the film inspector noticed either blurred copy because of movement during exposure, or duplicate copy. Unless we meant to delete copyrighted materials that should not have been filmed, you will find a good image of the page in the adjacent frame.

3. When a map, drawing or chart, etc., is part of the material being photographed the photographer has followed a definite method in "sectioning" the material. It is customary to begin filming at the upper left hand corner of a large sheet and to continue from left to right in equal sections with small overlaps. If necessary, sectioning is continued again—beginning below the first row and continuing on until complete.

4. For any illustrations that cannot be reproduced satisfactorily by xerography, photographic prints can be purchased at additional cost and tipped into your xerographic copy. Requests can be made to our Dissertations Customer Services Department.

5. Some pages in any document may have indistinct print. In all cases we have filmed the best available copy.

University
Microfilms
International

300 N. ZEEB ROAD, ANN ARBOR, MI 48106
18 BEDFORD ROW, LONDON WC1R 4EJ, ENGLAND

POWELL, DOUGLAS RAY

# THE CRYSTAL STRUCTURE DETERMINATIONS OF LUTETIUM(3)SULFIDE(4), NONSTOICHIOMETRIC NIOBIUM(1.06)SULFIDE(2), AND THREE GROUP-VIII COORDINATION COMPLEXES

*Iowa State University* PH.D. 1980

# The crystal structure determinations of $Lu_3S_4$, nonstoichiometric $Nb_{1.06}S_2$, and three Group VIII coordination complexes

by

Douglas Ray Powell

A Dissertation Submitted to the
Graduate Faculty in Partial Fulfillment of the
Requirements for the Degree of
DOCTOR OF PHILOSOPHY

Department: Chemistry
Major: Physical Chemistry

Approved:

Signature was redacted for privacy.

In Charge of Major Work

Signature was redacted for privacy.

For the Major Department

Signature was redacted for privacy.

For the Graduate College

Iowa State University
Ames, Iowa

1980

TABLE OF CONTENTS


| | Page |
|---|---|
| GENERAL INTRODUCTION | 1 |
| Explanation of Dissertation Format | 2 |
| SECTION I. THE CRYSTAL STRUCTURE OF $Lu_3S_4$ | 4 |
| Introduction | 4 |
| Experimental | 4 |
| Solution and Refinement | 7 |
| Discussion | 8 |
| SECTION II. THE CRYSTAL STRUCTURE OF 3-R $Nb_{1.06}S_2$ | 15 |
| Introduction | 15 |
| Experimental | 15 |
| Discussion | 18 |
| SECTION III. THE CRYSTAL AND MOLECULAR STRUCTURE OF BIS(δ-CAMPHORQUINONEDIOXIMATO)NICKEL(II) | 24 |
| Introduction | 24 |
| Experimental | 24 |
| Solution and Refinement | 26 |
| Discussion | 27 |
| SECTION IV. THE CRYSTAL AND MOLECULAR STRUCTURE OF THE HEXANUCLEAR COMPLEX $[Ni(\delta\text{-HCQD})_2 \cdot Ag]_3 \cdot 2\ 1/2\ CHCl_3$ | 43 |
| Introduction | 43 |
| Experimental | 43 |
| Solution and Refinement | 45 |
| Discussion | 47 |

| | Page |
|---|---|
| SECTION V. THE CRYSTAL AND MOLECULAR STRUCTURE OF CIS-DICHLOROBIS(METHYLDIPHENYLPHOSPHINITE)-PALLADIUM(II) | 65 |
| Introduction | 65 |
| Experimental | 66 |
| Solution and Refinement | 68 |
| Discussion | 69 |
| SUMMARY | 83 |
| REFERENCES | 84 |
| ACKNOWLEDGMENTS | 88 |
| APPENDIX: FOUR, A GENERAL CRYSTALLOGRAPHIC FOURIER PROGRAM | 89 |
| Introduction | 89 |
| General Description | 90 |
| Program Details | 97 |
| Conclusions | 103 |

# LIST OF TABLES


| | | Page |
|---|---|---|
| Table 1. | Final structural parameters for $Lu_3S_4$ | 9 |
| Table 2. | Final structural parameters for $3R\text{-}Nb_{1.06}S_2$ | 19 |
| Table 3. | Bond distances (Å) and angles (°) for 3-R $Nb_{1.06}S_2$ | 19 |
| Table 4. | Final structural parameters for $Ni(\delta\text{-HCQD})_2$ | 28 |
| Table 5. | Bond distances (Å) and angles (°) for $Ni(\delta\text{-HCQD})_2$ | 31 |
| Table 6. | Final structural parameters for $[Ni(\delta\text{-HCQD})_2Ag]_3$ | 48 |
| Table 7. | Bond distances (Å) and angles (°) for $[Ni(\delta\text{-HCQD})_2 \cdot Ag]_3$ | 53 |
| Table 8. | Least squares planes for $[Ni(\delta\text{-HCQD})_2 \cdot Ag]$ | 57 |
| Table 9. | Final structural parameters for $PdCl_2[P(OMe)Ph_2]_2$ | 70a |
| Table 10. | Bond distances (Å) and angles (°) for $PdCl_2[P(OMe)Ph_2]_2$ | 73 |
| Table 11. | Least squares planes for $PdCl_2[P(OMe)Ph_2]_2$ | 75 |

# LIST OF FIGURES


| | | Page |
|---|---|---|
| Figure 1. | Lutetium atom positions in $Lu_3S_4$ projected along the a axis. | 10 |
| Figure 2. | A view of 3-R $Nb_{1.06}S_2$ projected onto the $(11\bar{2}0)$ plane with the c axis vertical. | 20 |
| Figure 3. | A stereoscopic view of Ni(δ-HCQD)$_2$. | 33 |
| Figure 4. | A stereoscopic view of the unit cell of Ni(δ-HCQD)$_2$ projected along the c axis | 35 |
| Figure 5. | δ-Camphorquinone dioxime. | 37 |
| Figure 6. | Cis-Ni(δ-HCQD)$_2$. | 40 |
| Figure 7. | A stereoscopic view of [Ni(δ-HCQD)$_2$ · Ag]$_3$. | 58 |
| Figure 8. | A stereoscopic view of the unit cell of [Ni(δ-HCQD)$_2$ · Ag]$_3$ projected along the c axis. | 60 |
| Figure 9. | A stereoscopic view of $PdCl_2[P(OMe)Ph_2]_2$. | 77 |
| Figure 10. | A stereoscopic view of the unit cell of $PdCl_2[P(OMe)Ph_2]_2$ projected along the b axis. | 79 |
| Figure 11. | A block diagram of the program FOUR. | 98 |

# GENERAL INTRODUCTION

This dissertation reports the single crystal x-ray structure determinations of five selected inorganic compounds in order to help elucidate those features, at the molecular level, which would better explain their observed properties.

A new phase of metal-deficient lutetium monosulfide ($Lu_3S_4$) was recently studied by x-ray powder diffraction methods (1). The powder pattern of this phase exhibited all of the basic lines of the rock-salt structure monosulfide, with additional weak, low angle lines. A single crystal x-ray determination was undertaken to elucidate the structural basis for the superlattice reflections.

Layered transition metal dichalcogenides undergo intercalation reactions with electropositive species (2). Intercalation with alkali metals produces materials which have recently been used as cathodes in secondary batteries (3,4). One of these transition metal dichalcogenides, 3-R $Nb_{1.06}S_2$, was studied by single crystal x-ray techniques to gain a better understanding of the intercalation reaction on an atomic scale.

The infrared spectrum of bis(δ-camphorquinonedioximato) nickel (II), Ni(δ-HCQD)$_2$, exhibits bands at 1560 $cm^{-1}$ and 1690 $cm^{-1}$ (5,6). Although the former peak is typical of

nitrogen coordinated vic-dioxime complexes, the latter peak is at an unusually high frequency, uncharacteristic of such compounds (7). When $Ni(\delta\text{-HCQD})_2$ is reacted with silver nitrate, a product is formed in which the infrared band for $Ni(\delta\text{-HCQD})_2$ at 1690 $cm^{-1}$ has shifted to 1615 $cm^{-1}$ (8). The $Ni(\delta\text{-HCQD})_2$ complex reacts with Sm(III), La(III), and Hg(II) salts to produce compounds with infrared spectra similar to the $Ni(\delta\text{-HCQD})_2 \cdot Ag$ complex. Single crystal x-ray investigations of $Ni(\delta\text{-HCQD})_2$ and its silver nitrate reaction product were undertaken to establish the structural reasons for these unusual infrared spectra.

Recent studies show that palladium and platinum phosphine complexes catalyze hydrogenation (9) and alcohol carbonylation (10) reactions. Carboxylation of olefins may be catalyzed by metal phosphinite complexes (11). The structural parameters of one of these complexes, cis-dichlorobis(methyldiphenylphosphinite)palladium (II), were determined by single crystal x-ray techniques.

## Explanation of Dissertation Format

In this dissertation, the crystal and molecular structures of these five compounds are discussed in separate sections. Each section constitutes an adaptation of a separate journal article which either has been

published or is in preparation. Throughout this manuscript, the tables, figures, and references are numbered consecutively.

# SECTION I. THE CRYSTAL STRUCTURE OF $Lu_3S_4$

## Introduction

The monosulfide of lutetium loses metal preferentially upon vaporization in vacuo at 1750°C (1). Quenched samples were found to crystallize with the stoichiometry $Lu_3S_4$. The powder pattern of this phase exhibited all the cubic lines of the rock-salt structure monosulfide, with additional weak, low-angle lines. The lattice of $Lu_3S_4$ was tentatively established from Guinier data to be an orthorhombic superlattice derived from the parent face-centered cubic subcell (1). A similar superlattice has been previously reported for $Sc_2S_3$ (12). A single crystal study was undertaken to establish the detailed structure of this new phase.

## Experimental

Weak, low-angle data collected on a Guinier camera were indexed on a face-centered orthorhombic lattice with $\underline{a}$ = 10.8, $\underline{b}$ = 22.9, and $\underline{c}$ = 7.7Å. The orthorhombic cell was related to the parent cubic cell with $\underline{a}_{cub}$ = 5.355(1)Å by the relations $\underline{a}_{orth} = 2\ \underline{a}_{cub}$, $\underline{b}_{orth} = 3\sqrt{2}\ \underline{a}_{cub}$, and $\underline{c}_{orth} = \sqrt{2}\ \underline{a}_{cub}$ (1). A preliminary rotation photograph taken with a crystal aligned along one of the cubic axes, as indicated by the layer line spacings,

showed weak rows of diffraction maxima at 2/6, 3/6, and 4/6 of the cubic lattice layers. The cubic-to-orthorhombic transformation was used to index the weak, low-angle diffraction spots on the rotation photograph. The reflections at 3/6 of the cubic lattice could only be indexed if the crystal was assumed to be rotating around the cubic a axis; the reflections at 2/6 and 4/6 of the cubic lattice could only be indexed by assuming that the crystal was rotating around either the cubic b or c axes. However, no reflections could be found which could not be indexed via one of these assumptions. It is believed that, in the particular sample used for the rotation photograph, the orthorhombic supercell was disordered with respect to the cubic lattice. Several crystals of $Lu_3S_4$ were examined by film techniques, and all were found to crystallize in the disordered orthorhombic supercell or in the rock-salt structure with no supercell reflections.

A nearly spherical crystal (diameter 0.16 mm) was mounted and aligned on a four-circle diffractometer interfaced to a PDP-15 computer. The parent cubic lattice was found by an automatic indexing routine (13). The orthorhombic lattice was located by applying appropriate transformations and searching for the correct orientation of the superlattice; moreover, the superlattice of this sample was

not found to be disordered appreciably. Lattice constants $\underline{a}$ = 10.747(3), $\underline{b}$ = 22.813(6), and $\underline{c}$ = 7.602(2)Å, were determined from a least squares fit (14) to precise ± 2θ measurements of twelve strong, independent reflections ($2\theta > 30^{\circ}$) at 27°C using graphite-monochromated Mo $K_{\alpha}$ radiation ($\lambda$=0.71002Å).

Diffractometer data were collected at 27°C on an automated four-circle diffractometer designed and built in Ames Laboratory (15). All 4251 reflections within a 2θ sphere of 50° in the hkl, hk$\bar{l}$, h$\bar{k}$l, and h$\bar{k}\bar{l}$ octants were measured using an ω-stepscan technique.

As a general check on electronic and crystalline stability, three standard reflections were remeasured after every 75 reflections. These standards were not observed to vary significantly during the data collection period. The data were corrected for Lorentz and polarization effects. An absorption correction was applied assuming a spherical crystal ($\mu$=699.3 $cm^{-1}$). The estimated variance in each reflection was calculated by:

$$\sigma_I^2 = C_T + k_t C_B + (0.03C_T)^2 + (0.03C_B)^2$$

where $C_T$, $C_B$, and $k_t$ are the total count, the background count, and a counting time factor, respectively, and the factor 0.03 represents an estimate of nonstatistical errors. The estimated standard deviations in the structure factors

were calculated by the finite difference method (16). The observed ($F > 3\sigma_F$) data were averaged resulting in 140 unique reflections. The systematic absence of reflections with hkl, $h+k\neq 2n$, $k+l\neq 2n$, $l+h\neq 2n$ and 0kl, $k+l\neq 4n$; h0l, $l+h\neq 4n$; and hk0, $h+k\neq 4n$ uniquely determined the space group as $F_{ddd}$.

## Solution and Refinement

The data separated into two classes as a function of intensity. The strong data corresponded to the cubic sublattice. Hence, the similar cubic cell was used as a first approximation to the structure. The strong data were reindexed on the cubic lattice and averaged yielding 15 unique reflections. A structural model was refined by full matrix least squares techniques (17) to a final agreement factor $R = \Sigma \, ||F_o|-|F_c|| / \Sigma \, |F_o| = 0.050$ and a weighted agreement factor $R_\omega = ( \Sigma\omega(F_o-F_c)^2 / \Sigma\omega F_o^2 )^{\frac{1}{2}} = 0.059$. The function minimized was $\Sigma \, \omega||F_o|-|F_c||^2$ using weights of $1/\sigma_F^2$. The lutetium was placed at (0,0,0) with a multiplier of 0.75, and the sulfur was placed at (1/2,0,0) with a multiplier of 1.0. The final isotropic temperature factors were 0.78(17)Å$^2$ and 0.77(50)Å$^2$ for the metal and chalcogen, respectively.

This model was refined further using the full orthorhombic data set and the assumption that the supercell is

only a perturbation of the cubic cell. Correlation effects prohibited the simultaneous refinement of thermal parameters and lutetium atom multipliers. The thermal parameters were fixed at the values found in the cubic refinement. By cyclically varying three of the four metal atom multipliers at a time, convergence was found to be accelerated; only four cycles of refinement were required. All positional parameters and the lutetium multipliers were refined by full matrix least squares (17) to a final agreement factor R = 0.090 and weighted agreement factor $R_\omega$ = 0.140 using weights of $1/\sigma_F^2$ . The neutral atom scattering factors were from Hanson et al., (18) with corrections for anomalous dispersion effects (19). The final parameters are listed in Table 1. A drawing of the structure is shown in Figure 1.

## Discussion

The structure can be described in terms of occupation waves as follows: at a given height along a, (x = 0, 1/4, 1/2, or 3/4), the fractional occupancies in sequential (0 6 6 ) planes occur periodically in the order . . . 0.54, 0.75, 0.83, 0.84, 0.83, 0.75, 0.54 . . . . The occupation waves are in phase for x = 0 and x = 3/4 and for x = 1/4 and x = 1/2, and exactly out of phase for x = 0 and x = 1/4 (and thus for x = 1/2 and x = 3/4). Thus, the structure

Table 1. Final structural parameters for $Lu_3S_4$[a]

| Atom | Site Symmetry | Fractional Occupancy | x | y | z | B |
|---|---|---|---|---|---|---|
| Lu1 | 222 | 0.54(2) | 0.0 | 0.0 | 0.0 | 0.78 |
| Lu2 | 222 | 0.84(2) | 0.0 | 0.0 | 0.5 | 0.78 |
| Lu3 | 2 | 0.83(2) | 0.0 | 0.3326(1) | 0.0 | 0.78 |
| Lu4 | 2 | 0.75(2) | 0.0 | 0.1661(1) | 0.0 | 0.78 |
| S1 | 2 | 1.0 | 0.2498(16) | 0.0 | 0.0 | 0.77 |
| S2 | 1 | 1.0 | 0.2498(14) | 0.1663(3) | 0.0050(17) | 0.77 |

[a]In this table and subsequent tables, the values in parentheses denote the estimated standard deviations in the last digits.

Figure 1. Lutetium atom positions in $Lu_3S_4$ projected along the a axis.

Positions indicated by a single circle occur at x = 0 and x = 1/2, positions indicated by a double circle occur at x = 1/4 and x = 3/4. The (0,6,6) planes are indicated by the slanting lines and labeled A, B, C, and D. The sites have fractional occupancy as follows: A, 0.54 at x = 0, 3/4 and 0.84 at x = 1/4, 1/2; B, 0.75 at x = 0, 3/4 and 0.83 at x = 1/4, 1/2; C, 0.83 at x = 0, 3/4 and 0.75 at x = 1/4, 1/2; and D, 0.84 at x = 0, 3/4 and 0.54 at x = 1/4, 1/2.

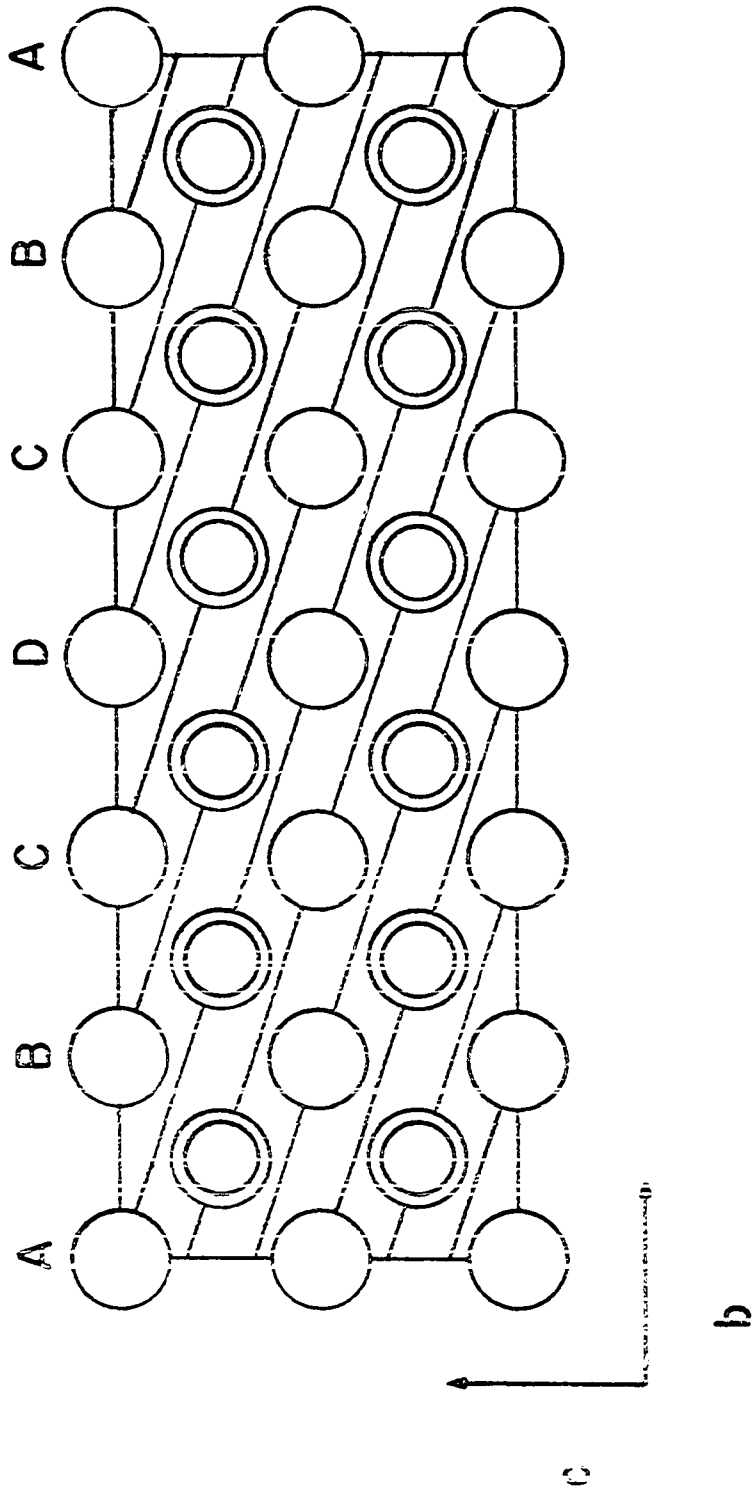
A
B
C
D
C
B
A
c
b

can be described as a sheared population wave defect ordering on the rock-salt type lattice.

Occupation waves have previously been observed in the Ti-S system by Wiegers and Jellinek (20). The phenomena of population wave structures are not understood from a fundamental point of view. Little is known as to the nature of the interactions that lead to such periodicities, nor are the underlying factors that yield a particular stoichiometry (S/Lu = 4/3 to a high degree of accuracy in this case) understood. These effects provide a fruitful area for theoretical investigation.

The lutetium contributions to the valence and conduction bands of lutetium sulfides are made up of $5d6s^2$ atomic levels, with $4f^{14}$ electrons remaining substantially localized (21). From this description, lutetium in these compounds may be considered as a transition metal. There are many similarities in the chemistry of lutetium and scandium compounds. All known sulfides of these metals from the monosulfide to the sesquisulfide are either of the rock-salt structure type or defect rock-salt type based upon a cubic closest-packed array of anions. It is interesting to examine the structure types encountered for various stoichiometries.

The monosulfides of both crystallize in the rock-salt structure. Lutetium sulfide retains the rock-salt structure

from the monosulfide to a stoichiometry of $LuS_{1.30}$ with random vacancies of the metal sites (1). In this work ($LuS_{1.33}$), the cations partially occupy the octahedral sites via the population waves described above. Lutetium sesquisulfide, $LuS_{1.5}$, is reported to crystallize in the $\alpha$-$Al_2O_3$ structure type (22), $R\bar{3}c$ with $\underline{a}$ = 6.722(2) and $\underline{c}$ = 18.160(3)Å. The corundum structure type ($\alpha$-$Al_2O_3$) is composed of a cubic closest-packed array of anions, similar to the rock-salt structure, but with the cations occupying two out of every three octahedral sites.

A broad stoichiometric range of $Sc_{1-x}S$ is reported (12). The vacancies partially order at low temperatures to yield the space group $R\bar{3}m$ with $\underline{a}$ = 3.657 and $\underline{c}$ = 17.91Å. The cation vacancies in these materials are randomly distributed in alternating (111) planes of the parent cubic sublattice. Scandium sesquisulfide has the defect rock-salt structure type (12), $F_{ddd}$ with $\underline{a}$ = 10.42, $\underline{b}$ = 22.10, and $\underline{c}$ = 7.37Å, in which the cations occupy two out of every three octahedral sites.

For lutetium and scandium sulfides, with stoichiometries between the monosulfide and the sesquisulfide, the metal vacancies are partially disordered over all octahedral sites. However, the metal vacancies of both sesquisulfides are ordered. The interchange of orthorhombic

and rhombohedral cells for corresponding stoichiometries of scandium and lutetium sulfides signifies a curious difference in the chemistry of these two metals.

# SECTION II. THE CRYSTAL STRUCTURE OF 3-R $Nb_{1.06}S_2$

## Introduction

Interest in transition metal chalcogenides has been recently sparked by the use of these materials as cathodes in secondary batteries (3,4). Cell reactions include the intercalation of $Li^+$ ions into the van der Waals layers of these materials. However, the intercalation reaction is inhibited by the presence of parent metal ions in these layers (23). In order to acquire a better structural understanding of such systems, a single crystal x-ray structure determination of 3-R $Nb_{1+x}S_2$ was undertaken. Although Morosin (24) has reported the single crystal structure 3-R $NbS_2$, only powder studies have been reported on the structure of the metal-rich 3-R $Nb_{1+x}S_2$ (25). Fisher and Sienko (26) have reported that the 3-R $Nb_{1+x}S_2$ polytype has a metal rich limit of $x = 0.17$. This stoichiometry corresponds to a $\underline{c}/\underline{a}$ ratio near which a charge density wave distortion is expected (27); however, no such distortion has ever been reported for this material.

## Experimental

A plate-shaped crystal (0.20 x 0.40 x 0.01 mm) was aligned and indexed (13) on a four-circle diffractometer

designed and built in this laboratory. Lattice constants, $\underline{a}$ = 3.3285(4) and $\underline{c}$ = 17.910(4)Å, were determined from a least-squares fit (14) to 13 strong, independent reflections measured at ±2θ (2θ > 25°) using graphite-monochromated Mo $K_\alpha$ radiation, λ = 0.70954Å. Reflections not meeting the condition -h+k+l=3n were the only systematic absences. This extinction condition is consistent with the space group $R_{3m}$. Neither axial oscillation photographs nor incremental step scans taken out the <10l>, <11l>, <h10>, and <hh0> lines showed any diffuse rings or supercell spots as reported by Boswell, Prodan, and Corbett (28).

Diffraction data were collected at room temperature using graphite monochromated Mo $K_\alpha$ radiation and the instrument described by Rohrbaugh and Jacobson (15). A total of 371 reflections were measured in the hkl, hk$\bar{l}$, h$\bar{k}$l, h$\bar{k}\bar{l}$ octants within a 2θ sphere of 60° using an ω-stepscan technique. Three reflections were periodically remeasured during the course of data collection, but they showed no significant decrease in intensity. The data were corrected for absorption (29) ($\mu$ = 63.0 $cm^{-1}$), Lorentz, and polarization effects. The estimated variance in each intensity was calculated by:

$$\sigma_I^2 = C_T + k_t C_B + (0.03\ C_T)^2 + (0.03\ C_B)^2 + (0.03\ C_N/A)^2$$

where $C_T$, $C_B$, $C_N$, $k_t$, and A are the total count, the background count, the net count, a counting time constant, and an absorption factor, respectively, and the factor 0.03 represents the estimate of nonstatistical errors. The estimated standard deviation in each structure factor was calculated by the finite difference method (16). The observed data ($F > 3\sigma_F$) were averaged yielding 79 independent reflections.

The symmetry of the space group $R_{3m}$ with Z=3 requires that the atoms be located at sites of 3m symmetry with coordinates of the form (0,0,z). The principal niobium (Nb1) was fixed at x = 0.0, and the sulfurs were initially input with the positions of Morosin (24). The sulfur positions, and all thermal parameters were refined by full matrix least squares (30) to a conventional crystallographic residual of R = 0.052. A difference map (31) indicated the presence of additional electron density between the van der Waals layers. Niobium (Nb2) was placed at this interstitial site with an occupancy factor of 0.1 and an isotropic thermal parameter identical to that of Nb1. All variables including the occupancy factors of both niobium atoms were refined by full matrix least squares (30) to a final conventional residual R = 0.026 and weighted residual $R_\omega$ = 0.031.

The function minimized was $\Sigma \omega||F_o|-|F_c||^2$ where $\omega = 1/\sigma_F^2$. Refinement using the inverse structure model yielded nearly identical results. The scattering factors used were those for $Nb^{4+}$ from Thomas and Umeda (32) and $S^{2-}$ from Tomiie and Stam (33) modified for anomalous dispersion effects (19). Unit occupancy of the sulfur atom sites was assumed. Refinement using neutral atom scattering factors (18) produced nearly identical structural parameters and a larger residual R = 0.030. Final structural parameters are listed in Table 2. A final difference map (31) revealed no peaks greater than 0.2 $e^-/A^3$. Selected bond distances and angles are listed in Table 3. A view of the cell is presented in Figure 2.

## Discussion

The distances and angles involving Nb1 and the sulfurs are in good agreement with those reported by Morosin (24). The sulfur-sulfur distances (3.311-3.443 A) indicate that the structure is made up of successive layers of closest-packed anions. The sulfurs form a trigonal prism around Nb1. In contrast, the sulfurs in the coordination environment of the van der Waals niobium, Nb2, comprise a distorted octahedron.

In the structure of stoichiometric $NbS_2$, the stacking sequence is . . . AbABcBCaC . . . where the capital letters

Table 2. Final structural parameters for 3R-$Nb_{1.06}S_2$

| Atom | Occupancy | x | $\beta_{11}$ | $\beta_{33}$ |
|---|---|---|---|---|
| Nb1 | 0.97(1) | 0.0 | 0.030(2) | 0.00156(4) |
| S1 | 1.0 | 0.2463(2) | 0.030(3) | 0.00129(10) |
| S2 | 1.0 | 0.4201(2) | 0.030(3) | 0.00140(11) |
| Nb2 | 0.09(1) | 0.8171(9) | 1.7(5) | |

Table 3. Bond distances (Å) and angles (°) for 3-R $Nb_{1.06}S_2$

| | | | |
|---|---|---|---|
| Nb1-S1 | 2.474(2) | Nb2-S1 | 2.577(11) |
| Nb1-S2 | 2.471(2) | Nb2-S2 | 2.234(8) |
| Nb1-Nb2 | 3.276(16) | S1 -S2 (same lamina) | 3.311(5) |
| Nb -Nb[a] | 3.3285(4) | S1 -S2 (interlamina) | 3.443(4) |
| S1 -Nb1-S1 | 84.53(6) | S1 -Nb2-S1 | 80.4(4) |
| S2 -Nb1-S2 | 84.65(6) | S2 -Nb2-S2 | 96.3(5) |
| S1 -Nb1-S2 | 78.00(9) | S1 -Nb2-S2 | 91.1(1) |
| S1 -Nb1-S2 | 134.27(3) | S1 -Nb2-S2 | 168.9(7) |
| Nb1-S1 -Nb2 | 81.0(3) | | |

[a]Unit cell translation.

Figure 2. A view of 3-R $Nb_{1.06}S_2$ projected onto the $(11\bar{2}0)$ plane with the $\underline{c}$ axis vertical.

The small and large circles represent niobium and sulfur atoms, respectively. The letters A, B, and C denote atoms with coordinates (0,0,z), (2/3,1/3,z), and (1/3, 2/3,z), respectively.

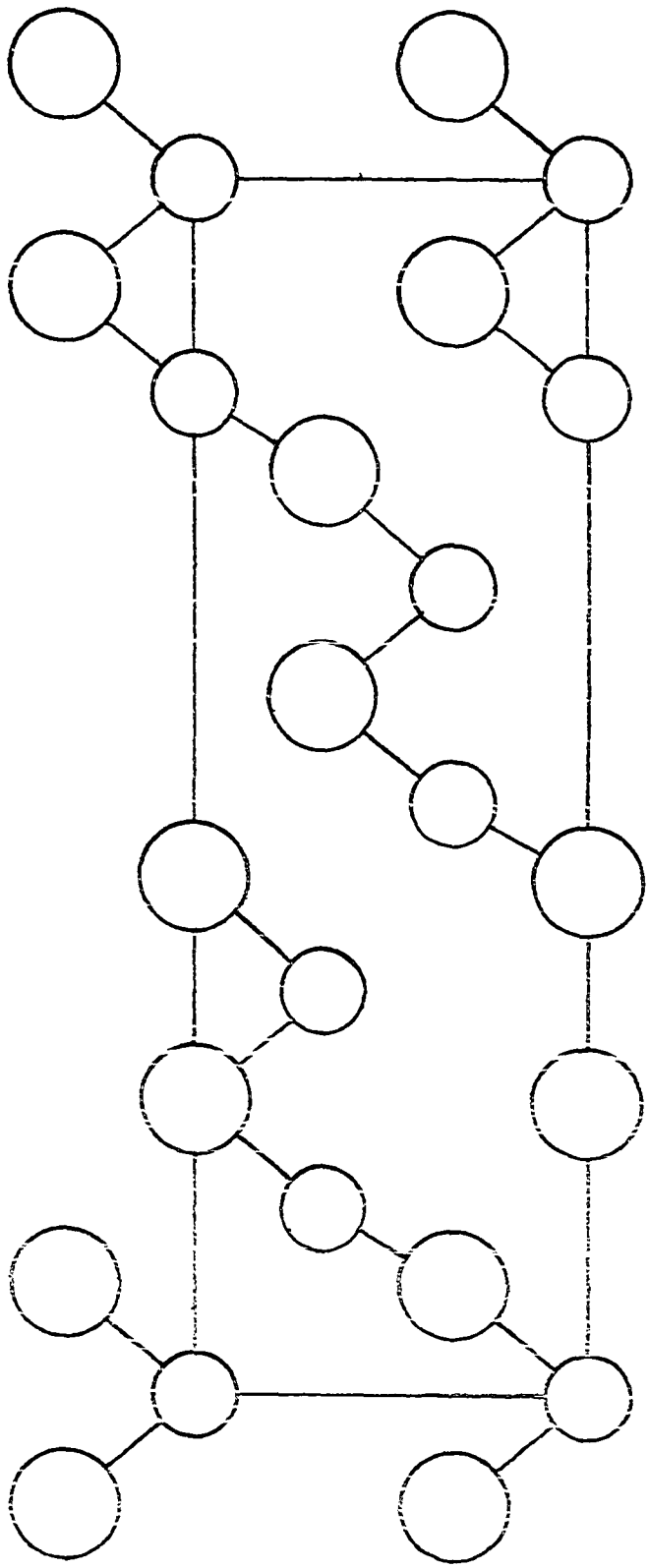
A
B
C

denote the sulfur sequence and the small letters denote the niobium sequence. The additional niobium atoms, designated by primed letters, go between the layers so as to give an octahedral arrangement yielding a stacking sequence . . . b'AbAc'BcBa'CaC . . . . These additional niobium atoms apparently move closer to one set of sulfurs in order to reduce repulsion effects from the Nb1 type atom directly over it, i.e., in the . . . Ac'BcB . . . arrangement, c' is closer to the A sulfur layer increasing the c'-c distance. The Nb2-S distances are 2.234 (8) and 2.577(11)Å, and the shortest Nb1-Nb2 distance is 3.276(16)Å. The niobium-niobium distance in a layer is 3.3285(4)Å.

It is also of some interest to examine coordination geometry via the concept of bond ionicity. The fractional ionicity $f_i$ as defined by Pauling (34) is 0.183 for niobium-sulfur bonds. Using the sulfur-sulfur separations in the (001) plane, the ionic radii for sulfur and Nb1 are 1.66 and 0.81Å, respectively. From Gamble's plot of the ratio of ionic radii versus the fractional ionic character of the metal-chalcogen bond (35), these data predict the observed trigonal prismatic coordination for Nb1. For Nb2, if the shorter niobium-sulfur bond length of 2.234Å is used, an effective metal radius of 0.57Å is obtained, also within the range predicted by Gamble for octahedral coordination.

Whittingham and Gamble (23) report a lattice expansion of 0.42Å in the c direction for the intercalation reaction of lithium with 3-R $NbS_2$, or 0.14Å per van der Waals layer. Although it is unclear how much confidence can be associated with the Nb2 radius as determined above, it is interesting to note that comparison to the $Li^+$ radius, approximately 0.7Å (34), would predict almost exactly the observed expansion.

# SECTION III. THE CRYSTAL AND MOLECULAR STRUCTURE OF BIS(δ-CAMPHORQUINONEDIOXIMATO)NICKEL(II)

## Introduction

Metal complexes of oxime ligands have been of interest for a number of years (36,37). These complexes have long been important in analytical chemistry (38). Also, these complexes have served as model compounds for kinetic studies of biologically important systems such as vitamin $B_{12}$ (39) and oxido-reductase (40). Previous studies of complexes with optically active ligands (41) have prompted this current study of bis(δ-camphorquinonedioximato)nickel(II), Ni(δ-HCQD)$_2$. Recently, the cobalt analog of this compound was reported to catalyze cyclopropanation reactions (42).

## Experimental

A tetrahedral shaped crystal, about 0.4 mm on an edge was mounted on a glass fiber and subsequently attached to an automated four-circle diffractometer. From five preliminary ω-oscillation photographs taken at various $\chi$ and $\phi$ settings, twelve independent reflections were selected and their coordinates were input to an automatic indexing algorithm (13). The resulting reduced cell and reduced cell scalars indicated orthorhombic symmetry.

This was confirmed by the mirror symmetry observed on oscillation photographs taken about all three axes. Layer line spacings were within experimental error of those predicted for this cell. A least squares fit (14) of the intensities ($\pm 2\theta$, $2\theta > 30^{\circ}$) of fifteen strong, independent reflections ($\pm 2\theta$), using Mo $K_{\alpha}$ radiation, $\lambda = 0.70954$Å, at $27^{\circ}$C, yielded $\underline{a}$ = 13.175(1), $\underline{b}$ = 13.652(2), and $\underline{c}$ = 12.031(3)Å.

Data were collected at room temperature on an automated four-circle diffractometer designed and built in this laboratory (15). The diffractometer is interfaced to a PDP-15 minicomputer in a time-sharing mode and is equipped with a scintillation counter. Graphite-monochromated Mo $K_{\alpha}$ radiation was used for data collection. All data (11562 reflections) within a $2\theta$ sphere of $60^{\circ}$ in the hkl, $\bar{h}$kl, h$\bar{k}$l, and hk$\bar{l}$ octants were collected using an $\omega$-stepscan technique. As a general check on electronic and crystal stability, the intensities of three standard reflections were remeasured every 75 reflections. These standard reflections did not significantly decrease during the data collection period. The intensity data were corrected for Lorentz and polarization effects. No absorption correction was deemed necessary ($\mu$=9.3 $cm^{-1}$). The estimated variance in each intensity was calculated by:

$$\sigma_I^2 = C_T + k_t C_B + (0.03\ C_T)^2 + (0.03\ C_B)^2$$

where $C_T$, $C_B$, and $k_t$ represent the total count, the background count, and a counting time factor, respectively; the factor 0.03 represents an estimate of nonstatistical errors. The estimated standard deviation in each structure factor was calculated by the finite difference method (16). The observed data ($I > 3\sigma_I$) were averaged yielding 2,253 independent reflections. The systematic absence of reflections with h00 , h≠2n; 0k0, k≠2n; and 00l, l≠2n uniquely determined the space group to be $P_{2_12_12_1}$.

## Solution and Refinement

The heavy atom was readily located on a Patterson map (31). All other nonhydrogen atoms were located by successive structure factor (30) and electron density map (31) calculations. Hydrogen atom positions were calculated assuming 1.07Å bonds and tetrahedral geometries. Full matrix least squares refinement (30) of positional and anisotropic thermal parameters for nonhydrogen atoms with fixed hydrogen positions yielded a conventional residual R=0.072 and a weighted residual $R_\omega$=0.094. A small secondary extinction effect was noted, and the observed data were corrected using a coefficient of $g=4.5 \times 10^{-7}$. Three cycles of full matrix least squares refinement yielded

a final residual R=0.066 and a weighted residual $R_\omega$=0.085. The function minimized was $\Sigma\ \omega||F_o|-|F_c||^2$ with weights of $\omega = 1/\sigma_F^2$. The metal scattering factors used were those for Ni(II) from Thomas and Umeda (32) corrected for anomalous dispersion effects (19). Scattering factors for the remaining nonhydrogen atoms were from Hanson et al., (18); hydrogen scattering factors were those of Stewart et al., (43). The final structural parameters are listed in Table 4, and the bond distances and angles are listed in Table 5. A stereographic view (44) of the molecule is shown in Figure 3, and a stereographic view (44) of the unit cell is illustrated in Figure 4.

## Discussion

The bidentate ligands form a square planar configuration around the nickel atom, coordinating to the metal via nitrogen and oxygen donor atoms rather than through N,N coordination common to other vic-dioxime ligands. This mode of coordination, which produces six-membered chelate rings, is believed to be due to the rigidity of the C=N bonds in the ligands (see Figure 5). The distances from Ni to O2, O4, N1, and N3 are 1.820(4), 1.840(3), 1.859(4), and 1.851(4)Å, respectively. The ligands form

Table 4. Final structural parameters for Ni(δ-HCQD)$_2$

(a) Final positional parameters (X $10^4$)

| Atom | x | y | z |
|---|---|---|---|
| Ni | | | |
| N1 | 887(3) | 1003(2) | - 229(4) |
| 01 | 631(3) | 1944(2) | 124(4) |
| 02 | 816(3) | - 944(3) | - 554(4) |
| N2 | 1778(3) | - 872(3) | -1020(4) |
| N3 | - 842(3) | -1053(3) | 449(4) |
| 03 | - 589(3) | -2000(2) | 160(4) |
| 04 | - 858(3) | 919(2) | 632(4) |
| N4 | -1734(4) | 812(4) | 1220(5) |
| C11 | 3207(4) | 215(4) | -1488(5) |
| C12 | 2172(3) | 0(3) | -1047(4) |
| C13 | 1747(4) | 931(4) | - 682(5) |
| C14 | 2566(4) | 1675(4) | - 901(5) |
| C15 | 3387(5) | 1450(5) | - 11(5) |
| C16 | 3836(4) | 448(5) | - 391(6) |
| C17 | 3048(4) | 1271(4) | -1959(5) |
| C18 | 2305(6) | 1246(6) | -2933(6) |
| C19 | 3991(5) | 1802(5) | -2303(6) |
| C10 | 3713(5) | - 546(5) | -2219(7) |
| C21 | -3011(4) | - 293(5) | 2068(6) |
| C22 | -2053(4) | - 50(4) | 1369(4) |
| C23 | -1673(4) | - 970(4) | 1024(5) |
| C24 | -2355(4) | -1752(4) | 1522(5) |
| C25 | -2145(6) | -1733(7) | 2781(7) |
| C26 | -2498(7) | - 794(8) | 3170(6) |
| C27 | -3353(5) | -1217(4) | 1492(5) |
| C28 | -3741(5) | -1048(7) | 309(6) |
| C29 | -4212(4) | -1768(5) | 2138(7) |
| C20 | -3747(6) | 520(6) | 2233(11) |

Table 4. Continued

(b) Final thermal parameters[a] ($\times 10^4$)

| Atom | $\beta_{11}$ | $\beta_{22}$ | $\beta_{33}$ | $\beta_{12}$ | $\beta_{13}$ | $\beta_{23}$ |
|---|---|---|---|---|---|---|
| Ni | 32.6(3) | 42.0(3) | 66.4(4) | -1.2(3) | 3.0(3) | -5.1(3) |
| N1 | 44(3) | 44(2) | 84(4) | 9(2) | 1(3) | - 8(3) |
| O1 | 83(3) | 41(2) | 176(5) | 4(2) | 45(4) | -24(3) |
| O2 | 42(2) | 59(2) | 142(4) | -14(2) | 25(3) | -28(3) |
| N2 | 50(3) | 50(3) | 131(5) | 0(2) | 33(3) | -22(3) |
| N3 | 39(2) | 45(2) | 95(4) | - 5(2) | 8(3) | - 9(3) |
| O3 | 65(3) | 43(2) | 168(5) | - 5(2) | 41(3) | -21(3) |
| O4 | 51(2) | 46(2) | 112(4) | 0(2) | 32(3) | - 5(2) |
| N4 | 52(3) | 60(3) | 119(5) | 0(3) | 25(3) | -13(3) |
| C11 | 46(3) | 62(4) | 101(5) | - 7(3) | 23(3) | -10(4) |
| C12 | 37(2) | 54(3) | 76(4) | - 5(3) | 5(3) | -14(3) |
| C13 | 46(3) | 43(3) | 78(4) | - 1(2) | 8(3) | - 2(3) |
| C14 | 68(4) | 49(3) | 99(5) | - 8(3) | 31(4) | - 2(3) |
| C15 | 66(4) | 102(5) | 92(5) | -29(4) | 18(4) | -39(5) |
| C16 | 40(3) | 101(5) | 130(7) | - 7(3) | - 2(4) | - 4(5) |
| C17 | 54(4) | 62(4) | 78(4) | 4(3) | 18(3) | 3(3) |
| C18 | 118(7) | 123(7) | 97(6) | - 5(6) | 3(6) | 17(6) |
| C19 | 81(4) | 73(4) | 125(7) | -11(4) | 41(5) | 0(5) |
| C10 | 94(5) | 82(5) | 145(7) | 17(4) | 42(6) | -42(5) |
| C21 | 72(4) | 64(4) | 137(7) | -11(3) | 63(5) | -14(4) |
| C22 | 51(3) | 53(3) | 86(4) | - 4(3) | 18(3) | 2(4) |
| C23 | 40(3) | 51(3) | 72(4) | - 1(2) | 2(3) | - 3(3) |
| C24 | 50(3) | 59(4) | 102(5) | - 3(3) | 12(4) | 13(4) |

[a]The $\beta ij$ are defined by: $T = \exp -(h^2\beta_{11} + k^2\beta_{22} + l^2\beta_{33} + 2hk\beta_{12} + 2hl\beta_{13} + 2kl\beta_{23})$.

Table 4. Continued

| Atom | $\beta_{11}$ | $\beta_{22}$ | $\beta_{33}$ | $\beta_{12}$ | $\beta_{13}$ | $\beta_{23}$ |
|---|---|---|---|---|---|---|
| C25 | 86(5) | 125(7) | 112(7) | -40(5) | -15(5) | 44(7) |
| C26 | 133(8) | 180(10) | 69(5) | -81(8) | 12(5) | -19(6) |
| C27 | 54(3) | 63(4) | 100(5) | 1(3) | 10(4) | 9(4) |
| C28 | 75(5) | 171(8) | 105(7) | -36(6) | -21(5) | 34(7) |
| C29 | 53(4) | 75(4) | 161(8) | -10(3) | 29(5) | 4(5) |
| C20 | 113(7) | 68(5) | 431(21) | -13(5) | 155(11) | -23(9) |

Table 5. Bond distances (Å) and angles (°) for $Ni(\delta\text{-HCQD})_2$

(a) Bond distances

| | | | |
|---|---|---|---|
| Ni - N1 | 1.859(4) | C11 - C16 | 1.590(9) |
| Ni - O2 | 1.820(4) | C11 - C17 | 1.563(8) |
| Ni - N3 | 1.851(4) | C14 - C17 | 1.525(8) |
| Ni - O4 | 1.840(3) | C17 - C18 | 1.527(10) |
| N1 - O1 | 1.396(5) | C17 - C19 | 1.497(8) |
| N2 - O2 | 1.388(6) | C11 - C10 | 1.517(8) |
| N3 - O3 | 1.380(5) | C21 - C22 | 1.553(7) |
| N4 - O4 | 1.362(6) | C22 - C23 | 1.414(7) |
| N1 - C13 | 1.261(6) | C23 - C24 | 1.519(7) |
| N2 - C12 | 1.300(6) | C24 - C25 | 1.540(10) |
| N3 - C23 | 1.301(6) | C25 - C26 | 1.442(12) |
| N4 - C22 | 1.264(7) | C21 - C26 | 1.639(11) |
| C11 - C12 | 1.492(6) | C21 - C27 | 1.507(8) |
| C12 - C13 | 1.457(7) | C24 - C27 | 1.505(7) |
| C13 - C14 | 1.505(7) | C27 - C28 | 1.530(9) |
| C14 - C15 | 1.553(9) | C27 - C29 | 1.565(8) |
| C15 - C16 | 1.559(9) | C21 - C20 | 1.488(9) |
| O1 - O4 | 2.486(5) | O2 - O3 | 2.498(6) |

(b) Bond angles

| | | | |
|---|---|---|---|
| N1 - Ni - O2 | 93.9(2) | C13 - C14 - C17 | 101.5(4) |
| N1 - Ni - N3 | 175.6(2) | C15 - C14 - C17 | 102.4(4) |
| N1 - Ni - O4 | 86.2(2) | C11 - C17 - C18 | 110.1(5) |
| O2 - Ni - N3 | 85.9(2) | C11 - C17 - C19 | 115.8(5) |
| O2 - Ni - O4 | 173.0(2) | C11 - C17 - C14 | 95.0(4) |
| N3 - Ni - O4 | 94.2(2) | C18 - C17 - C19 | 109.3(5) |
| Ni - N1 - O1 | 118.8(3) | C14 - C17 - C18 | 112.5(5) |
| Ni - N1 - C13 | 126.3(3) | C14 - C17 - C19 | 113.7(5) |
| Ni - O2 - N2 | 131.1(3) | C17 - C11 - C10 | 118.8(5) |
| O1 - N1 - C13 | 114.8(4) | C27 - C21 - C20 | 119.4(6) |
| O2 - N2 - C12 | 116.1(4) | C21 - C22 - C23 | 104.9(4) |
| N1 - C13 - C12 | 122.9(5) | C22 - C23 - C24 | 107.4(4) |
| N1 - C13 - C14 | 131.9(5) | C23 - C24 - C25 | 105.7(5) |
| N2 - C12 - C11 | 123.7(5) | C24 - C25 - C26 | 106.0(7) |
| N2 - C12 - C13 | 129.6(4) | C25 - C26 - C21 | 103.9(6) |
| C11 - C12 - C13 | 106.6(4) | C22 - C21 - C26 | 101.0(5) |
| C12 - C13 - C14 | 105.1(4) | C22 - C21 - C27 | 100.0(5) |

Table 5. Continued

| | | | |
|---|---|---|---|
| C13 - C14 - C15 | 104.2(4) | C22 - C21 - C20 | 116.2(6) |
| C14 - C15 - C16 | 103.6(5) | C26 - C21 - C27 | 98.4(6) |
| C15 - C16 - C11 | 102.8(5) | C26 - C21 - C20 | 118.2(8) |
| C12 - C11 - C16 | 102.7(4) | C23 - C24 - C27 | 99.6(4) |
| C12 - C11 - C17 | 100.8(4) | C25 - C24 - C27 | 99.9(6) |
| C12 - C11 - C10 | 118.2(5) | C21 - C27 - C28 | 113.7(6) |
| C16 - C11 - C17 | 100.7(5) | C21 - C27 - C29 | 113.0(5) |
| C16 - C11 - C10 | 112.9(5) | C21 - C27 - C24 | 97.7(5) |
| C28 - C27 - C29 | 107.0(6) | N3 - C23 - C22 | 122.1(5) |
| C24 - C27 - C28 | 112.8(6) | O4 - N4 - C22 | 117.1(5) |
| C24 - C27 - C29 | 112.7(5) | O3 - N3 - C23 | 114.7(4) |
| N4 - C22 - C23 | 132.0(5) | Ni - O4 - N4 | 129.6(3) |
| N4 - C22 - C21 | 123.1(5) | Ni - N3 - C23 | 124.8(4) |
| N3 - C23 - C24 | 130.3(5) | Ni - N3 - O3 | 120.4(3) |

Figure 3. A stereoscopic view of $Ni(\delta\text{-HCQD})_2$.

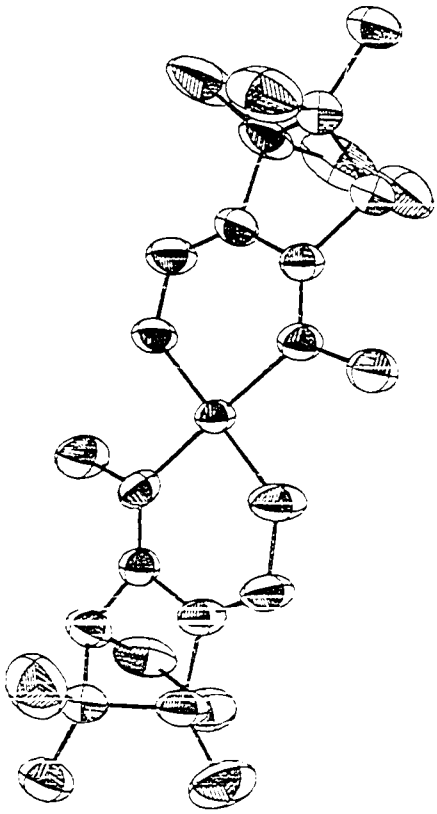

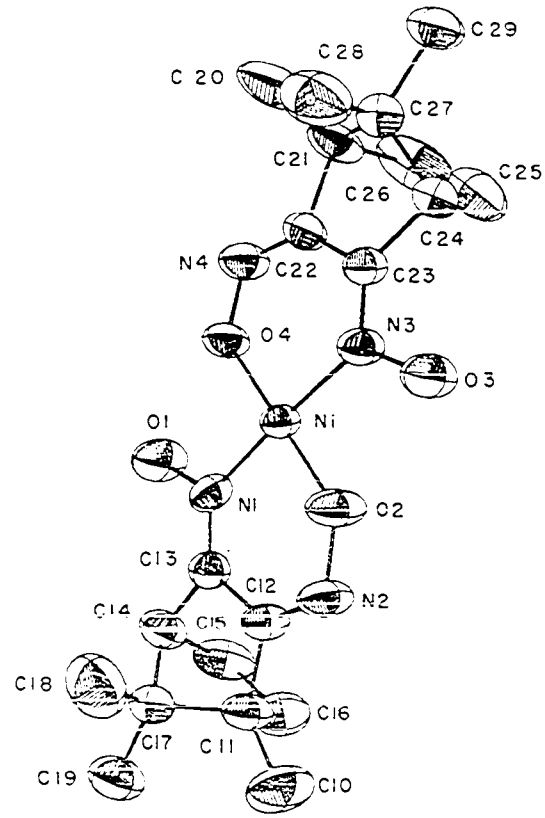
C29
C28
C 20
C27
C21
C25
C26
C24
N4
C22
C23
O4
N3
O3
O1
Ni
N1
O2
C13
C12
N2
C14
C15
C18
C16
C17
C11
C19
C10

Figure 4. A stereoscopic view of the unit cell of $Ni(\delta\text{-HCQD})_2$ projected along the c axis.

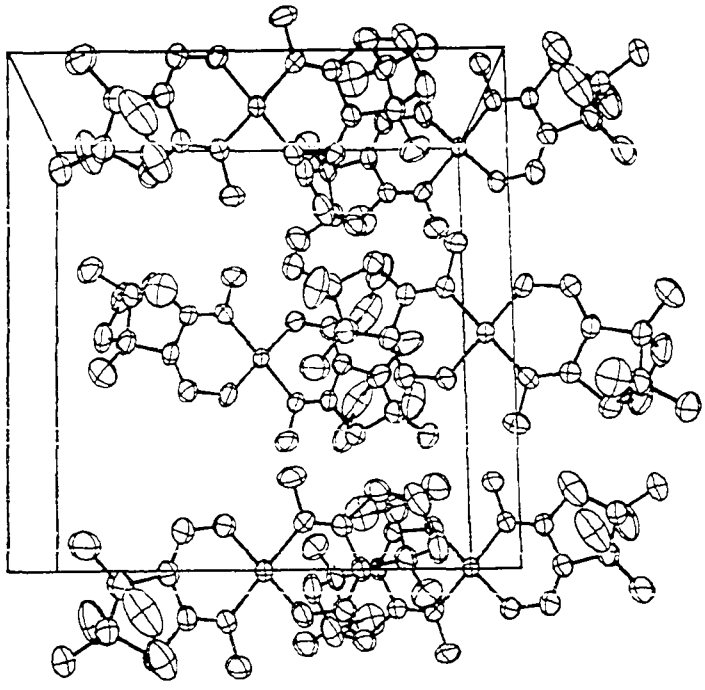

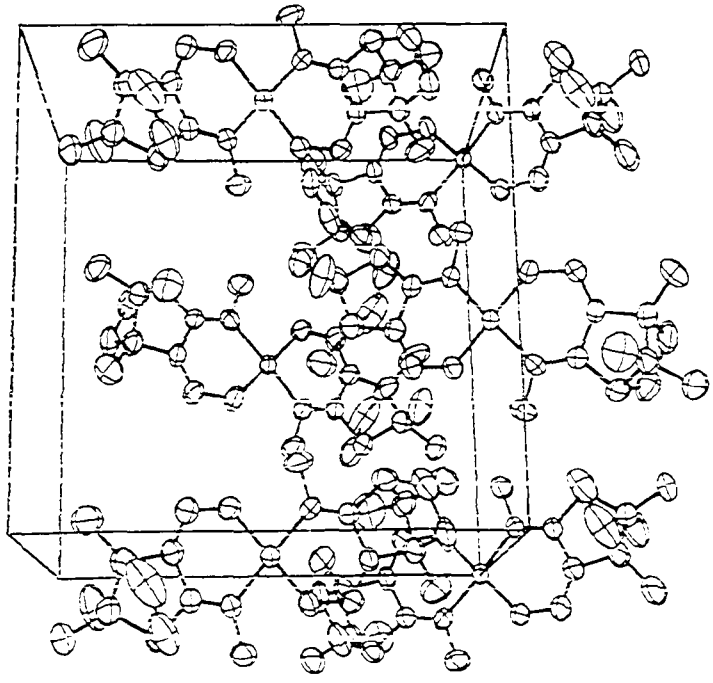

Figure 5. δ-Camphorquinone dioxime.

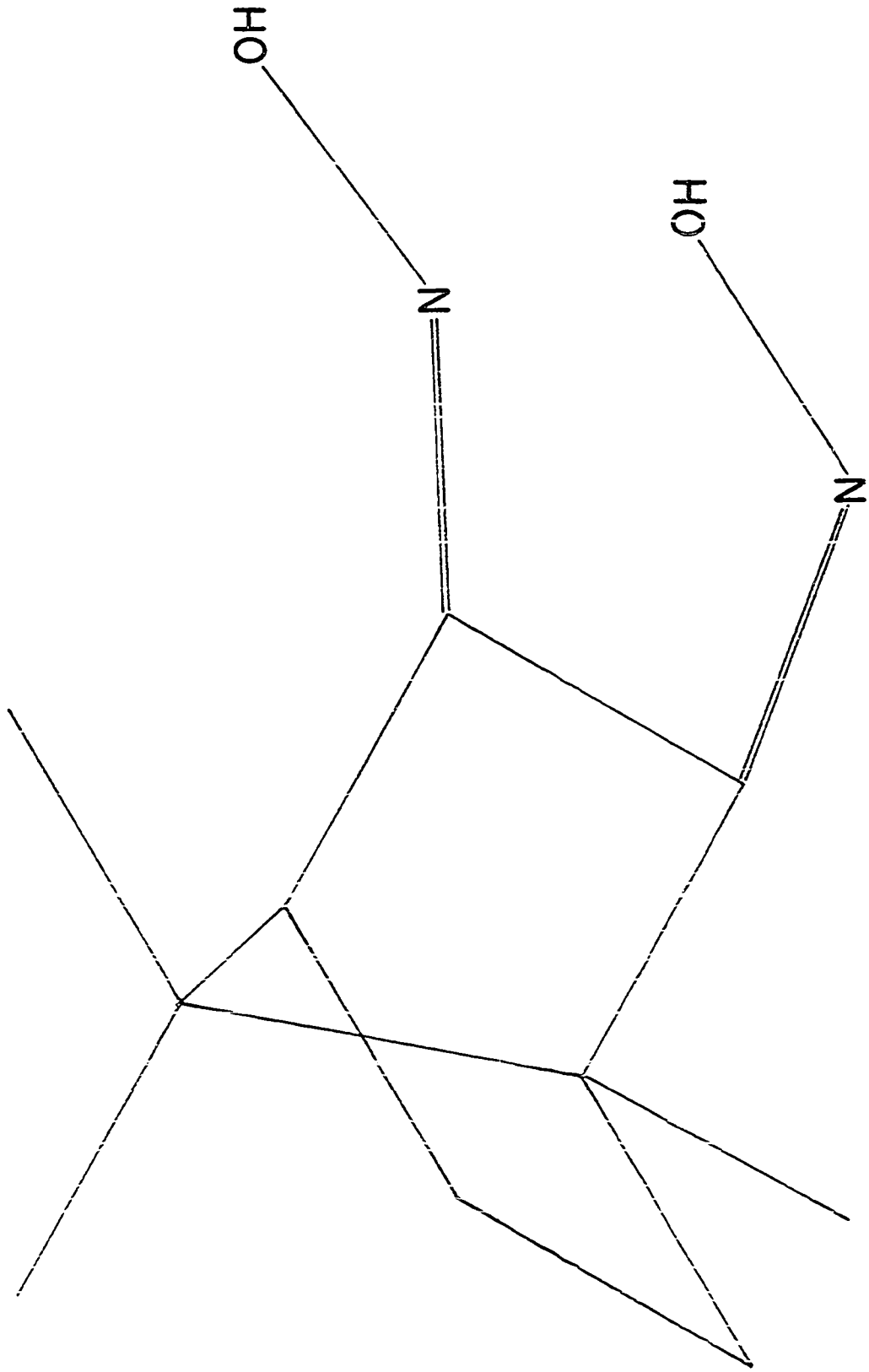
HO
N
HO
N

angles around the metal of N1-Ni-O2 93.9(2)°, N3-Ni-O4 94.2(2)°, N1-Ni-O4 86.2(2)°, and N3-Ni-O2 85.9(2)°. The four atoms coordinated to the metal are ±0.052Å from a least squares plane of these atoms (0.4496x - 0.1073y + 0.8868z = 0.0827). The Ni-N1-O2 plane and the Ni-N3-O4 plane form an angle of 4.62°.

In addition to metal-ligand bonding, the complex is stabilized by intramolecular hydrogen bonds. The two ligands and the metal form two stereochemically equivalent, five-membered, hydrogen-bonded chelate rings. If the ligands were to bond to the metal in a cis configuration (see Figure 6), they would form four- and six-membered, hydrogen-bonded chelate rings. The hydrogen-bonded oxygens, O1-O4 and O2-O3, are 2.486(5) and 2.498(6)Å apart. There are no intermolecular hydrogen bonds. The molecules pack in the unit cell such that the shortest distance between metal atoms is 8.932Å, precluding any metal-metal interactions as occur in the dimethylglyoximato complex $Ni(HDMG)_2$ (45).

The infrared spectrum of $Ni(\delta\text{-HCQD})_2$ taken in a KBr pellet shows absorption peaks at 1560 $cm^{-1}$ and 1690 $cm^{-1}$ (5,6). Although the former peak is typical of nitrogen coordinated α-dioxime complexes, the latter peak is at an unusually high frequency, uncharacteristic of such compounds (7). Deuteration studies indicate that the band is

Figure 6. Cis-Ni(δ-HCQD)$_2$.

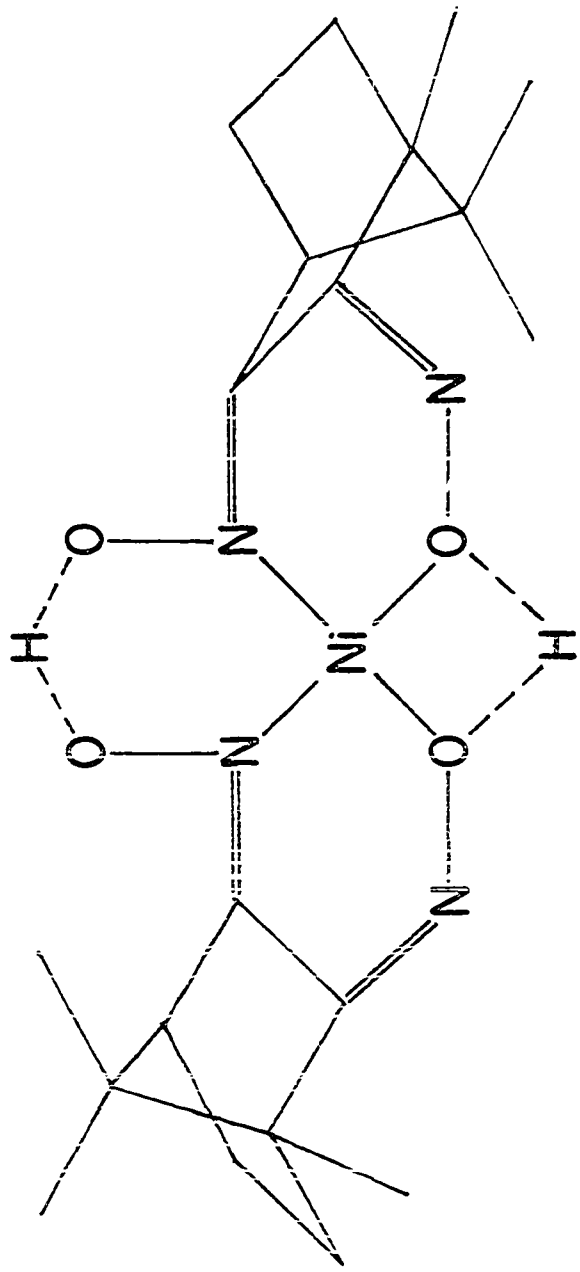
N
O
N
O
H
Ni
H
O
N
O
N

not associated with the OH groups but presumably arises from a vibration which has considerable C=N stretching character. This combination of absorption bands may allow easy identification of other complexes containing vic-dioxime ligands coordinated through nitrogen and oxygen atoms.

# SECTION IV. THE CRYSTAL AND MOLECULAR STRUCTURE OF THE HEXANUCLEAR COMPLEX $[Ni(\delta\text{-HCQD})_2 \cdot Ag]_3 \cdot 2\ 1/2\ CHCl_3$

## Introduction

The reaction of bis(δ-camphorquinonedioximato)-nickel(II), $Ni(\delta\text{-HCQD})_2$, with silver nitrate in a mixed chloroform, water, and methanol solvent produces neutral molecular species with one silver per nickel complex. The infrared spectrum of the reaction product in a KBr pellet no longer shows an absorption band at 1690 $cm^{-1}$ corresponding to the oxygen-coordinated oxime ν (C=N) vibration found in $Ni(\delta\text{-HCQD})_2$ (5,6). Instead a new band is observed at 1615 $cm^{-1}$ (8). A single crystal x-ray study was undertaken to determine the nature of this reaction product. The palladium analog of $Ni(\delta\text{-HCQD})_2$ reacts with silver nitrate to produce a similar product (8). Also the $Ni(\delta\text{-HCQD})_2$ complex reacts with Sm(III), La(III), Nd(III), and Hg(II) salts to produce compounds with infrared spectra similar to the $Ni(\delta\text{-HCQD})_2 \cdot Ag$ complex (8).

## Experimental

A green single crystal of approximate dimensions 0.36 x 0.19 x 0.16 mm was selected and mounted directly on an automated four-circle diffractometer. Twelve

independent reflections taken from four preliminary $\omega$-oscillation photographs at various $\chi$ and $\phi$ settings were input to an automatic indexing algorithm (13). The resulting reduced cell and reduced cell scalars indicated orthorhombic symmetry. Subsequent axial oscillation photographs confirmed the mmm symmetry. The lattice constants ($\underline{a}$ = 15.990(5), $\underline{b}$ = 38.44(1), and $\underline{c}$ = 13.437(5) Å) were obtained from a least squares fit (14) of the precisely measured $\pm 2\theta$ valves of thirteen independent reflections ($2\theta > 20^{\circ}$) at 25°C using graphite-monochromated $MoK_{\alpha}$ radiation ($\lambda$=0.70954Å).

Intensity data were collected at 25°C on an automated, four-circle diffractometer designed and built in this laboratory (15). Graphite-monochromated Mo $K_{\alpha}$ radiation was used for data collection. All data (4412 reflections) within a $2\theta$ sphere of $40^{\circ}$ in the hkl octant were measured using an $\omega$-stepscan technique.

As a general check on electronic and crystal stability, the intensities of three standard reflections were measured every seventy-five reflections. These standards indicated considerable decay in the last 1037 data. The decay, as measured from the standard reflections, was found by least squares methods to fit a quadratic polynomial: $y(x) = 5979 + (-0.2615)x + (-0.0007267)x^2$, where x and y are,

respectively, the reflection number and the net intensity. All data collected after the first 3375 reflections were divided by $\frac{y(x)}{y(0)} = 1.0 + (-0.4374 \times 10^{-5})x + (-1.216 \times 10^{-7})x^2$ to correct for decay.

The intensity data were then corrected for Lorentz and polarization effects. Although the linear absorption coefficient, $\mu$, was 14.47 $cm^{-1}$, no absorption correction was deemed necessary because the data was collected only to $40^{\circ}$ in $2\theta$ and because the transmittance was $0.80 \pm 0.09$. The estimated error in each intensity was found by:

$$\sigma_I^2 = C_T + k_t C_B + (0.03\ C_T)^2 + (0.03\ C_B)^2$$

where $C_T$, $C_B$, and $k_t$ represent the total count, the background count, and a counting time constant respectively, and the factor of 0.03 represents an estimate of nonstatistical errors. The error in each structure factor was calculated by the finite difference method (16). A total of 3021 observed ($I > 3\sigma_I$) reflections were retained for structural solution and refinement. The systematic absence of reflections with h00, h≠2n; 0k0, k≠2n; and 00l, l≠2n uniquely determined the space group to be $P_{2_12_12_1}$.

## Solution and Refinement

The positions of the Ag atoms were obtained from an analysis of a sharpened three-dimensional Patterson map (31).

The remaining nonhydrogen atoms, including disordered solvent atoms were found by successive structure factor (17) and electron density map calculations (31). Hydrogen positions were calculated using 1.07Å bond distances and tetrahedral geometries and included in subsequent structure factor calculations but were not refined. Atomic positional parameters, anisotropic thermal parameters for the metal atoms, and isotropic thermal parameters for the remaining nonhydrogen atoms in the hexanuclear molecule were refined by block matrix least squares methods (17) to a conventional residual R=0.107 and weighted residual $R_\omega$ =0.127. The function minimized was $\Sigma\ \omega||F_o|-|F_c||^2$ with weights $\omega=1/\sigma_F{}^2$. There were three possible solvent sites in the structure. Although two of the solvent sites exhibited peaks corresponding to disordered $CHCl_3$ molecules, the third site contained much less electron density. The refined structure contained less solvent than was indicated by elemental analysis, which is believed due to some loss of solvent during data collection. The decay observed in the standard reflections is consistent with the assumption of solvent loss. Thermal and occupancy factors for the solvent atoms were estimated from successive difference maps. The final electron density difference map revealed no peaks larger than 1.0 $e^-/Å^3$. The scattering factors for Ag(I) and Ni(II) were those of Thomas and Umeda (32). The

scattering factors for the remaining nonhydrogen atoms were those of Hanson et al., (18). The metal scattering factors and those for chlorine were modified for anomalous dispersion effects (19). Hydrogen scattering factors were those of Stewart et al., (43). The final positional and thermal parameters are listed in Table 6. Bond distances and angles are listed in Table 7; least squares planes are listed in Table 8. Stereoscopic views (44) of the cluster complex and the unit cell are illustrated in Figures 7 and 8, respectively.

## Discussion

The unit cell consists of four hexanuclear molecules with $CHCl_3$ molecules occupying interstitial sites. Each hexanuclear molecule consists of three $Ni(\delta\text{-HCQD})_2^-$ groups coordinated to a linear chain of three silver atoms. The δ-camphorquinone dioximato ligands coordinate to the Ni(II) atoms via nitrogen and oxygen donor atoms forming six-membered chelate rings. However, unlike the trans configuration found for the simple $Ni(\delta\text{-HCQD})_2$ complex, the ligands bond to the nickel atoms in a cis configuration. Several interesting features of the structure are discussed below.

The linear chain of silver atoms produces an unusual

Table 6. Final structural parameters for $[Ni(\delta\text{-HCQD})_2Ag]_3$

(a) Final positional parameters[a] for $[Ni(\delta\text{- HCQD})_2Ag]_3$

| Atom | x | y | z | B |
|---|---|---|---|---|
| Ag1 | 0.2093(2) | 0.1705(1) | -0.0952(3) | |
| Ag2 | 0.3188(2) | 0.1124(1) | -0.1801(3) | |
| Ag3 | 0.4230(2) | 0.0530(1) | -0.2658(3) | |
| Ni1 | 0.4713(4) | 0.1239(2) | 0.0159(5) | |
| Ni2 | 0.1326(4) | 0.0568(2) | -0.1905(5) | |
| Ni3 | 0.3937(4) | 0.1704(2) | -0.3759(4) | |
| 101 | 0.4422(18) | 0.0951(7) | -0.0944(23) | 5.0(7) |
| 102 | 0.6331(19) | 0.1170(8) | 0.1003(25) | 6.2(8) |
| 103 | 0.5524(21) | 0.1625(9) | 0.1716(26) | 7.4(9) |
| 104 | 0.3700(19) | 0.1418(8) | -0.0279(23) | 5.3(7) |
| 1N1 | 0.4795(23) | 0.0620(10) | -0.1228(29) | 5.4(9) |
| 1N2 | 0.5747(25) | 0.1038(9) | 0.0399(29) | 5.6(9) |
| 1N3 | 0.4795(23) | 0.1588(9) | 0.1187(29) | 5.0(9) |
| 1N4 | 0.3152(22) | 0.1676(9) | 0.0088(26) | 5.2(8) |
| 1C10 | 0.5666(37) | 0.0005(15) | -0.1742(46) | 7.9(16) |
| 1C11 | 0.5987(27) | 0.0218(11) | -0.0934(34) | 5.0(10) |
| 1C12 | 0.5451(29) | 0.0515(13) | -0.0769(36) | 4.9(12) |
| 1C13 | 0.5972(27) | 0.0710(11) | 0.0084(32) | 4.6(10) |
| 1C14 | 0.6786(33) | 0.0491(14) | 0.0180(40) | 6.3(13) |

[a]The isotropic thermal parameters are listed for all nonmetal atoms.

Table 6. Continued

| Atom | x | y | z | B |
|---|---|---|---|---|
| 1C15 | 0.6392(35) | 0.0198(14) | 0.0848(44) | 7.7(15) |
| 1C16 | 0.5909(32) | 0.0020(13) | 0.0047(39) | 6.4(13) |
| 1C17 | 0.6834(38) | 0.0359(15) | -0.0830(48) | 7.5(16) |
| 1C18 | 0.7012(34) | 0.0579(14) | -0.1699(43) | 7.3(14) |
| 1C19 | 0.7529(33) | 0.0062(13) | -0.0904(40) | 6.9(13) |
| 1C20 | 0.1959(34) | 0.2097(14) | 0.1276(42) | 6.9(14) |
| 1C21 | 0.2937(33) | 0.2093(13) | 0.1471(39) | 6.3(13) |
| 1C22 | 0.3422(28) | 0.1816(12) | 0.0903(36) | 5.9(11) |
| 1C23 | 0.4188(27) | 0.1793(10) | 0.1414(30) | 4.3(10) |
| 1C24 | 0.4175(31) | 0.2034(12) | 0.2243(36) | 5.2(12) |
| 1C25 | 0.4248(35) | 0.2382(14) | 0.1791(43) | 8.4(14) |
| 1C26 | 0.3418(29) | 0.2432(12) | 0.1119(37) | 5.5(12) |
| 1C27 | 0.3221(28) | 0.2037(12) | 0.2568(34) | 4.8(11) |
| 1C28 | 0.2953(32) | 0.1685(14) | 0.2991(39) | 6.4(13) |
| 1C29 | 0.2920(42) | 0.2307(17) | 0.3259(53) | 9.4(19) |
| 201 | 0.2441(17) | 0.0572(7) | -0.2207(20) | 4.2(6) |
| 202 | 0.0350(24) | 0.0006(10) | -0.2628(30) | 7.5(10) |
| 203 | -0.0342(22) | 0.0353(9) | -0.1395(27) | 8.4(10) |
| 204 | 0.1677(16) | 0.1016(7) | -0.1442(20) | 4.5(7) |
| 2N1 | 0.2948(22) | 0.0339(9) | -0.2699(28) | 5.2(9) |
| 2N2 | 0.1167(20) | 0.0143(8) | -0.2601(25) | 5.5(9) |
| 2N3 | 0.0271(23) | 0.0614(10) | -0.1374(28) | 3.9(8) |
| 2N4 | 0.1224(23) | 0.1269(9) | -0.1081(29) | 4.9(9) |
| 2C10 | 0.3948(33) | -0.0268(13) | -0.3559(39) | 6.3(13) |
| 2C11 | 0.2986(31) | -0.0229(12) | -0.3757(38) | 6.0(12) |
| 2C12 | 0.2535(28) | 0.0089(11) | -0.3081(36) | 4.5(11) |
| 2C13 | 0.1661(28) | -0.0011(12) | -0.3125(38) | 5.0(11) |
| 2C14 | 0.1602(30) | -0.0351(12) | -0.3694(37) | 5.3(12) |

Table 6. Continued

| Atom | x | y | z | B |
|---|---|---|---|---|
| 2C15 | 0.1790(34) | -0.0217(14) | -0.4662(42) | 7.6(14) |
| 2C16 | 0.2642(39) | -0.0143(15) | -0.4752(48) | 8.7(17) |
| 2C17 | 0.2388(37) | -0.0522(16) | -0.3372(46) | 8.4(16) |
| 2C18 | 0.2574(42) | -0.0868(16) | -0.4012(53) | 9.2(18) |
| 2C19 | 0.2474(34) | -0.0628(14) | -0.2316(42) | 7.4(15) |
| 2C20 | 0.0064(33) | 0.1843(13) | -0.0426(41) | 6.4(14) |
| 2C21 | -0.0207(34) | 0.1459(14) | -0.0266(41) | 6.8(14) |
| 2C22 | 0.0456(30) | 0.1213(13) | -0.0818(38) | 5.7(12) |
| 2C23 | -0.0004(26) | 0.0882(11) | -0.0871(33) | 4.1(10) |
| 2C24 | -0.0959(29) | 0.0944(11) | -0.0466(35) | 5.0(11) |
| 2C25 | -0.0732(38) | 0.0948(14) | 0.0663(45) | 8.5(16) |
| 2C26 | -0.0207(35) | 0.1328(14) | 0.0836(43) | 6.8(14) |
| 2C27 | -0.1014(34) | 0.1357(13) | -0.0798(41) | 6.1(14) |
| 2C28 | -0.1003(32) | 0.1389(12) | -0.1850(39) | 6.2(13) |
| 2C29 | -0.1834(37) | 0.1483(15) | -0.0230(45) | 8.5(16) |
| 301 | 0.4007(18) | 0.1247(7) | -0.3379(21) | 4.8(7) |
| 302 | 0.5043(19) | 0.1934(8) | -0.5306(24) | 5.7(8) |
| 303 | 0.4149(22) | 0.2343(8) | -0.4723(25) | 6.8(8) |
| 304 | 0.3154(18) | 0.1706(8) | -0.2693(22) | 5.2(7) |
| 3N1 | 0.4524(22) | 0.0974(9) | -0.3632(28) | 5.2(9) |
| 3N2 | 0.4751(20) | 0.1645(8) | -0.4718(24) | 3.7(8) |
| 3N3 | 0.3720(19) | 0.2162(8) | -0.4004(24) | 3.2(7) |
| 3N4 | 0.2671(23) | 0.1947(10) | -0.2356(28) | 4.7(9) |
| 3C10 | 0.5395(34) | 0.0397(14) | -0.4584(42) | 6.7(14) |
| 3C11 | 0.5639(28) | 0.0762(11) | -0.4849(33) | 4.5(10) |
| 3C12 | 0.4991(28) | 0.1057(12) | -0.4437(36) | 4.9(11) |
| 3C13 | 0.5107(36) | 0.1379(14) | -0.4916(43) | 6.5(15) |

Table 6. Continued

| Atom | x | y | z | B |
|---|---|---|---|---|
| 3C14 | 0.5769(30) | 0.1313(11) | -0.5723(34) | 5.2(11) |
| 3C15 | 0.6617(31) | 0.1254(13) | -0.5082(38) | 6.1(13) |
| 3C16 | 0.6442(33) | 0.0913(14) | -0.4515(41) | 5.9(14) |
| 3C17 | 0.5593(36) | 0.0953(14) | -0.5972(46) | 7.7(15) |
| 3C18 | 0.4772(33) | 0.0913(13) | -0.6463(40) | 7.4(14) |
| 3C19 | 0.6206(32) | 0.0758(13) | -0.6605(39) | 6.4(13) |
| 3C20 | 0.1713(38) | 0.2504(16) | -0.1438(45) | 9.4(17) |
| 3C21 | 0.2108(26) | 0.2565(10) | -0.2434(32) | 3.9(10) |
| 3C22 | 0.2678(27) | 0.2237(11) | -0.2734(34) | 4.9(11) |
| 3C23 | 0.3136(30) | 0.2354(12) | -0.3633(36) | 5.6(12) |
| 3C24 | 0.2921(30) | 0.2748(12) | -0.3695(37) | 5.6(12) |
| 3C25 | 0.2035(41) | 0.2728(16) | -0.4115(52) | 9.8(18) |
| 3C26 | 0.1468(30) | 0.2599(12) | -0.3211(38) | 5.9(12) |
| 3C27 | 0.2739(33) | 0.2838(13) | -0.2640(41) | 6.6(14) |
| 3C28 | 0.3526(36) | 0.2812(15) | -0.1931(45) | 7.8(15) |
| 3C29 | 0.2323(33) | 0.3215(14) | -0.2598(42) | 7.4(14) |
| 1Cl1(0.4)[b] | 0.5515(27) | 0.2176(12) | -0.2676(34) | 7.0 |
| 1Cl2(0.4) | 0.6120(22) | 0.1534(9) | -0.2148(26) | 7.0 |
| 1Cl3(0.4) | 0.5810(24) | 0.2004(9) | -0.0690(28) | 7.0 |
| 1Cl4(0.25) | 0.6242(31) | 0.1758(13) | -0.1071(40) | 7.0 |
| 1Cl5(0.25) | 0.5138(32) | 0.2174(13) | -0.0980(41) | 7.0 |
| 1Cl6(0.25) | 0.5787(34) | 0.2081(14) | -0.2846(40) | 7.0 |
| 1Cs1(0.4) | 0.5533(73) | 0.1934(30) | -0.1930(95) | 7.0 |

[b]Only about 1.3 $CHCl_3$ was observed on an electron denisty difference map. Elemental analyses indicated 2 1/2 $CHCl_3$ molecules.

Table 6. Continued

| Atom | x | y | z | B |
|---|---|---|---|---|
| 1C12(0.4) | 0.1438(21) | 0.1527(9) | -0.4040(26) | 7.0 |
| 2C13(0.4) | 0.1095(21) | 0.0815(9) | -0.4340(26) | 7.0 |
| 2C14(0.25) | 0.0774(34) | 0.1022(13) | -0.3785(41) | 7.0 |
| 2C15(0.25) | 0.2171(37) | 0.0922(15) | -0.4421(45) | 7.0 |
| 2C16(0.25) | 0.1378(36) | 0.1528(14) | -0.4734(43) | 7.0 |
| 2CS2(0.25) | 0.1383(121) | 0.1171(51) | -0.4164(152) | 7.0 |
| 1OS(0.55) | 0.5187(37) | 0.3270(16) | -0.3466(44) | 7.0 |

(b) Anisotropic thermal parameters (X $10^5$) of the heavy atoms[c]

| | $\beta_{11}$ | $\beta_{22}$ | $\beta_{33}$ | $\beta_{12}$ | $\beta_{13}$ | $\beta_{23}$ |
|---|---|---|---|---|---|---|
| Ag1 | 396(18) | 69(3) | 805(29) | 3(6) | -48(20) | 18(9) |
| Ag2 | 400(16) | 58(3) | 718(26) | 0(6) | 24(19) | 32(8) |
| Ag3 | 411(17) | 67(3) | 793(29) | 0(7) | -41(21) | 24(8) |
| Ni1 | 390(30) | 58(5) | 709(47) | -6(11) | 8(34) | -2(14) |
| Ni2 | 404(30) | 55(5) | 676(45) | -7(10) | -44(33) | 18(14) |
| Ni3 | 429(31) | 57(5) | 633(44) | 13(11) | -55(31) | -2(14) |

[c]The $\beta ij$ are defined by: $T = \exp -(h^2\beta_{11} + k^2\beta_{22} + l^2\beta_{33} + 2hk\beta_{12} + 2hl\beta_{13} + 2kl\beta_{23})$ .

Table 7. Bond distances (Å) and angles (°) for $[Ni(\delta\text{-HCQD})_2 \cdot Ag]_3$

(a) Distances and angles between metal atoms

| | | | |
|---|---|---|---|
| Ag1 - Ag2 | 3.059(5) | Ag2 - Ag3 | 3.052(7) |
| Ag2 - Ni1 | 3.616(7) | Ag2 - Ni2 | 3.668(8) |
| Ag2 - Ni3 | 3.651(8) | | |
| Ag1 - Ag2 - Ag3 | 178.1(2) | Ni1 - Ag2 - Ni2 | 130.3(2) |
| Ni1 - Ag2 - Ni3 | 103.2(2) | Ni2 - Ag2 - Ni3 | 126.5(2) |

(b) Interatomic distances for $[Ni(\delta\text{-HCQD})_2 \cdot Ag]_3$

| | Ni1 | Ni2 | Ni3 |
|---|---|---|---|
| Ag1 - N4 | 2.20(4) | 2.18(4) | 2.30(4) |
| Ag1 - O4 | 2.94(3) | 2.81(3) | 2.89(3) |
| Ag2 - O4 | 2.48(3) | 2.50(3) | 2.54(3) |
| Ag2 - O1 | 2.38(3) | 2.50(3) | 2.54(3) |
| Ag3 - O1 | 2.83(3) | 2.93(3) | 2.94(3) |
| Ag3 - N1 | 2.15(4) | 2.18(4) | 2.20(4) |
| M[a] - O1 | 1.91(3) | 1.83(3) | 1.89(3) |
| M - O4 | 1.86(3) | 1.92(3) | 1.90(3) |
| M - N2 | 1.85(4) | 1.90(3) | 1.85(3) |
| M - N3 | 1.93(4) | 1.84(4) | 1.82(3) |
| O2 - O3 | 2.38(5) | 2.40(5) | 2.26(4) |
| O1 - O4 | 2.31(4) | 2.34(4) | 2.41(4) |
| O1 - N1 | 1.46(5) | 1.38(4) | 1.38(4) |
| O4 - N4 | 1.41(5) | 1.31(4) | 1.29(5) |
| N2 - O2 | 1.34(5) | 1.41(5) | 1.44(4) |
| N3 - O3 | 1.37(5) | 1.40(5) | 1.37(5) |
| N1 - C12 | 1.28(6) | 1.27(6) | 1.35(6) |

[a]M corresponds to the metal atoms labelled at the top of each column.

Table 7. Continued

| | Ni1 | Ni2 | Ni3 |
|---|---|---|---|
| N4 - C22 | 1.29(6) | 1.30(6) | 1.22(6) |
| N2 - C13 | 1.38(6) | 1.21(6) | 1.20(6) |
| N3 - C23 | 1.29(6) | 1.31(6) | 1.29(6) |
| C10 - C11 | 1.45(8) | 1.57(7) | 1.50(7) |
| C11 - C12 | 1.44(6) | 1.68(7) | 1.63(6) |
| C11 - C16 | 1.53(7) | 1.48(8) | 1.48(7) |
| C11 - C17 | 1.46(7) | 1.56(8) | 1.68(8) |
| C12 - C13 | 1.60(6) | 1.45(6) | 1.41(7) |
| C13 - C14 | 1.56(7) | 1.52(7) | 1.54(7) |
| C14 - C15 | 1.57(8) | 1.43(8) | 1.62(7) |
| C14 - C17 | 1.45(8) | 1.48(8) | 1.45(7) |
| C15 - C16 | 1.49(8) | 1.40(8) | 1.54(7) |
| C17 - C18 | 1.47(8) | 1.61(8) | 1.48(8) |
| C17 - C19 | 1.60(8) | 1.48(8) | 1.50(8) |
| C20 - C21 | 1.59(8) | 1.55(7) | 1.50(7) |
| C21 - C22 | 1.52(7) | 1.60(7) | 1.61(6) |
| C21 - C26 | 1.58(7) | 1.56(8) | 1.47(6) |
| C21 - C27 | 1.56(7) | 1.53(8) | 1.48(6) |
| C22 - C23 | 1.41(6) | 1.47(6) | 1.48(6) |
| C23 - C24 | 1.45(6) | 1.64(6) | 1.56(6) |
| C24 - C25 | 1.47(7) | 1.46(8) | 1.53(8) |
| C24 - C27 | 1.59(7) | 1.65(7) | 1.49(7) |
| C25 - C26 | 1.62(7) | 1.70(8) | 1.60(8) |
| C27 - C28 | 1.53(7) | 1.42(8) | 1.58(8) |
| C27 - C29 | 1.47(8) | 1.59(8) | 1.60(7) |

(c) Bond angles for $[Ni(\delta\text{-HCQD})_2 \cdot Ag]$

| | Ni1 | Ni2 | Ni3 |
|---|---|---|---|
| O1 - Ag2 - O4 | 56.9(10) | 55.8(9) | 56.8(9) |
| Ag2 - O4 - M | 112.4(14) | 111.7(12) | 109.7(13) |

Table 7. Continued

| | Ni1 | Ni2 | Ni3 |
|---|---|---|---|
| Ag2 - O1 - M | 114.6(13) | 115.2(13) | 112.3(13) |
| O1 - M - O4 | 75.9(13) | 77.2(12) | 80.5(13) |
| O1 - M - N2 | 96.4(15) | 91.6(13) | 91.9(13) |
| O4 - M - N3 | 91.6(15) | 93.2(14) | 90.4(14) |
| N2 - M - N3 | 96.0(16) | 98.7(16) | 97.3(14) |
| O1 - M - N3 | 167.4(14) | 168.3(15) | 170.7(15) |
| O4 - M - N2 | 171.3(16) | 166.5(13) | 172.0(14) |
| M - O1 - N1 | 127.6(24) | 132.4(23) | 134.2(24) |
| M - O4 - N4 | 133.7(25) | 128.9(23) | 131.4(27) |
| M - N2 - O2 | 124.8(27) | 177.3(25) | 121.1(23) |
| M - N3 - O3 | 120.0(27) | 124.3(28) | 121.4(24) |
| M - N2 - C13 | 124.1(31) | 128.2(31) | 126.4(35) |
| M - N3 - C23 | 123.0(31) | 125.7(31) | 128.3(30) |
| O1 - N1 - C12 | 119.0(38) | 112.3(34) | 110.4(32) |
| N1 - C12 - C13 | 128.5(43) | 135.7(43) | 130.2(44) |
| N1 - C12 - C11 | 131.3(45) | 122.8(39) | 117.2(37) |
| N2 - C13 - C12 | 120.8(38) | 118.3(42) | 125.8(52) |
| N2 - C13 - C14 | 133.5(40) | 132.3(42) | 128.6(48) |
| O2 - N2 - C13 | 110.6(35) | 114.0(36) | 112.4(38) |
| C11 - C12 - C13 | 99.8(36) | 101.4(36) | 111.8(40) |
| C12 - C13 - C14 | 104.0(36) | 108.0(38) | 105.6(42) |
| C13 - C14 - C15 | 95.7(38) | 97.8(40) | 103.0(38) |
| C14 - C15 - C16 | 97.1(43) | 110.9(49) | 103.3(38) |
| C15 - C16 - C11 | 110.6(41) | 103.8(50) | 110.0(42) |
| C12 - C11 - C16 | 102.3(36) | 99.5(39) | 100.1(36) |
| C12 - C11 - C17 | 104.0(40) | 94.7(38) | 88.5(33) |
| C12 - C11 - C10 | 110.5(41) | 113.4(38) | 113.8(38) |
| C16 - C11 - C17 | 100.7(41) | 103.4(43) | 98.0(38) |
| C16 - C11 - C10 | 109.6(40) | 122.6(45) | 121.4(42) |
| C17 - C11 - C10 | 127.3(46) | 118.3(42) | 127.7(40) |
| C13 - C14 - C17 | 99.0(42) | 100.5(41) | 100.8(41) |
| C15 - C14 - C17 | 107.7(45) | 104.3(44) | 98.7(38) |
| C11 - C17 - C14 | 99.8(46) | 95.9(43) | 101.6(42) |
| C18 - C17 - C19 | 103.1(46) | 105.5(48) | 106.0(46) |
| O4 - N4 - C22 | 112.4(34) | 120.2(36) | 120.2(38) |
| N4 - C22 - C23 | 132.6(42) | 127.2(43) | 128.2(42) |
| N4 - C22 - C21 | 123.0(41) | 130.9(44) | 127.2(40) |
| N3 - C23 - C22 | 125.4(39) | 122.5(40) | 119.9(40) |
| N3 - C23 - C24 | 125.8(41) | 126.8(37) | 134.1(43) |

Table 7. Continued

| | Ni1 | Ni2 | Ni3 |
|---|---|---|---|
| O3 - N3 - C23 | 117.0(36) | 109.8(35) | 110.1(33) |
| C21 - C22 - C23 | 104.0(39) | 101.7(38) | 104.3(34) |
| C22 - C23 - C24 | 108.8(38) | 108.9(35) | 103.3(37) |
| C23 - C24 - C25 | 105.2(40) | 96.2(37) | 100.1(40) |
| C24 - C25 - C26 | 105.8(41) | 104.8(41) | 105.2(48) |
| C25 - C26 - C21 | 97.7(37) | 98.5(41) | 100.0(40) |
| C22 - C21 - C26 | 100.3(38) | 104.4(41) | 106.7(35) |
| C22 - C21 - C27 | 103.2(39) | 101.0(41) | 97.0(34) |
| C28 - C27 - C29 | 107.3(43) | 117.5(46) | 111.6(42) |
| C26 - C21 - C27 | 104.7(39) | 111.1(44) | 106.2(38) |
| C27 - C21 - C20 | 116.4(42) | 114.5(40) | 124.4(42) |
| C25 - C24 - C27 | 100.5(39) | 105.4(37) | 100.5(43) |
| N2 - O2 - O3 | 98.3(24) | 101.7(25) | 98.1(22) |
| N3 - O3 - O2 | 100.1(25) | 95.1(25) | 101.9(22) |

Table 8. Least squares planes[a] for $[Ni(\delta\text{-HCQD})_2 \cdot Ag]$

| Atom | D[b] | Atom | D |
|---|---|---|---|
| | Plane 1: Ni1-101-104-1N2-1N3<br>0.4553x + 0.6283y + 0.6308z - 6.3268 = 0 | | |
| Ni1 | -0.0377 | 1N2 | 0.0261 |
| 101 | -0.0102 | 1N3 | -0.0064 |
| 104 | 0.0283 | | |
| | Plane 2: Ni2-201-204-2N2-2N3<br>-0.2591x + 0.4619y + 0.8482z - 2.636 = 0 | | |
| Ni2 | -0.0059 | 2N2 | 0.0986 |
| 201 | -0.01165 | 2N3 | -0.0924 |
| 204 | 0.1163 | | |
| | Plane 3: Ni3-301-304-3N2-3N3<br>0.7150x + 0.2574y - 0.6500z - 2.9148 = 0 | | |
| Ni3 | -0.0102 | 3N2 | -0.0245 |
| 301 | -0.0225 | 3N3 | -0.0191 |
| 304 | 0.0274 | | |
| | Plane 4: Ni1-Ni2-Ni3-Ag2<br>0.5494x - 0.7432y + 0.3818z - 0.5180 = 0 | | |
| Ni1 | 0.0013 | Ni3 | 0.0012 |
| Ni2 | 0.0016 | Ag2 | -0.0043 |

[a]Planes are defined as $C_1x + C_2y + C_3z + C_4 = 0$ where x, y, and z are Cartesian coordinates.

[b]D = distance (Å) of the given atom from the fitted plane.

Figure 7. A stereoscopic view of $[Ni(\delta\text{-HCQD})_2 \cdot Ag]_3$.

The thermal ellipsoids are drawn at the 50% and 10% probability levels for the metal and nonmetal atoms, respectively.

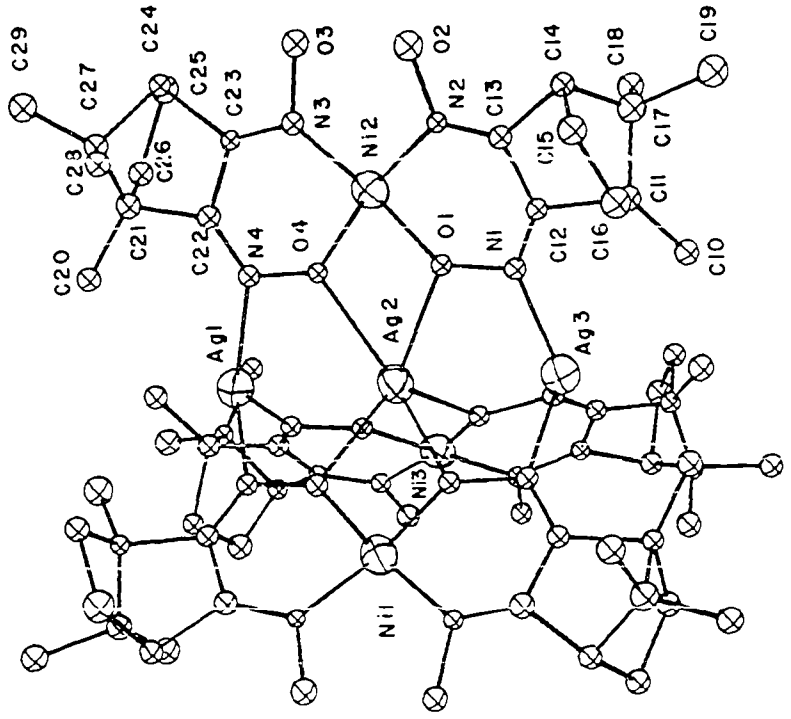
C29
C27
C24
C25
C23
O3
N3
Ni2
O2
N2
C13
C14
C18
C19
C28
C26
C15
C17
C21
C22
N4
O4
O1
Ni
C12
C16
C11
C20
C10
Ag1
Ag2
Ag3
Ni3
Ni1

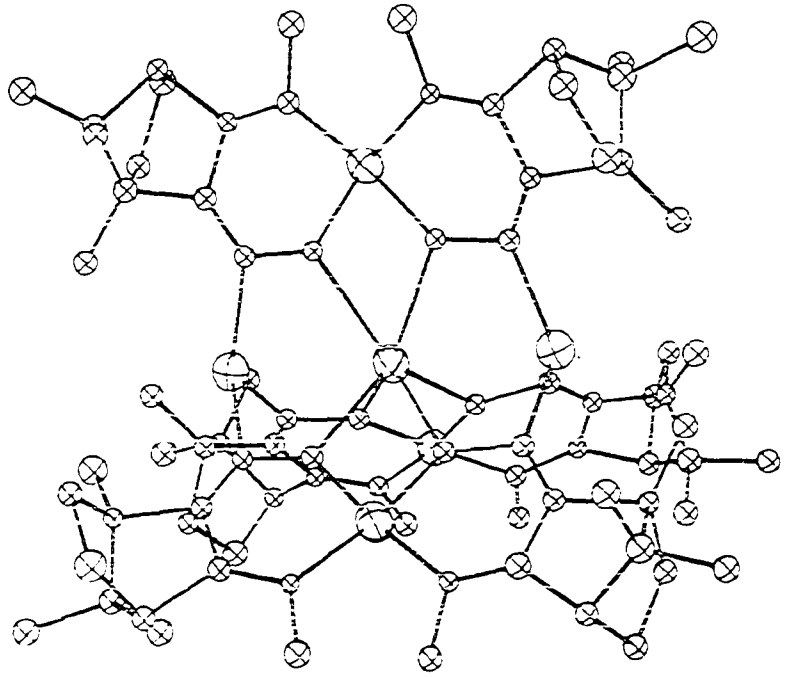

Figure 8. A stereoscopic view of the unit cell of $[Ni(\delta\text{-HCQD})_2 \cdot Ag]_3$ projected along the c axis.

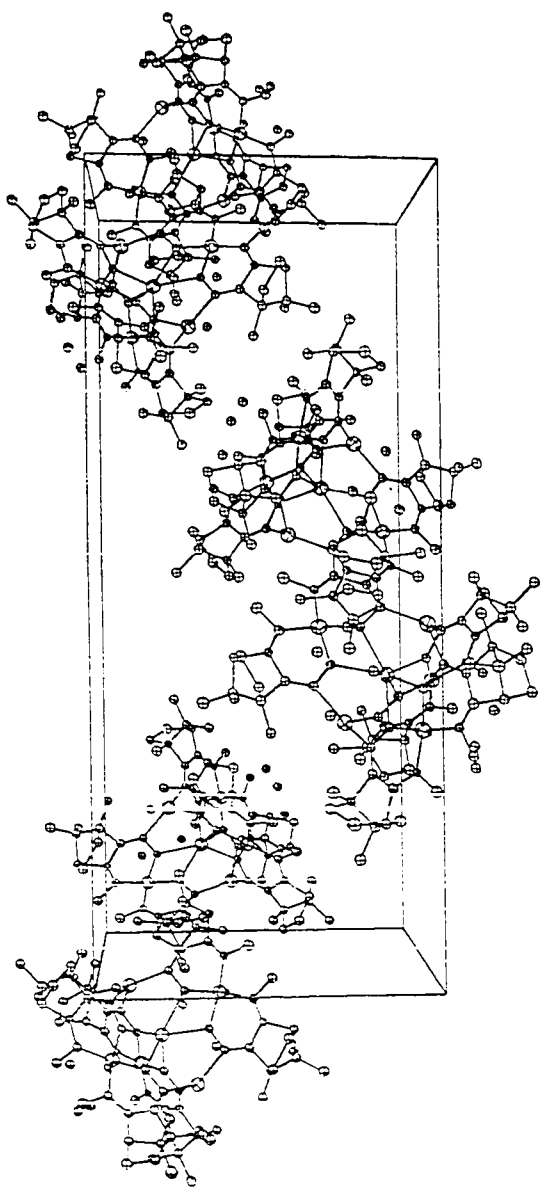

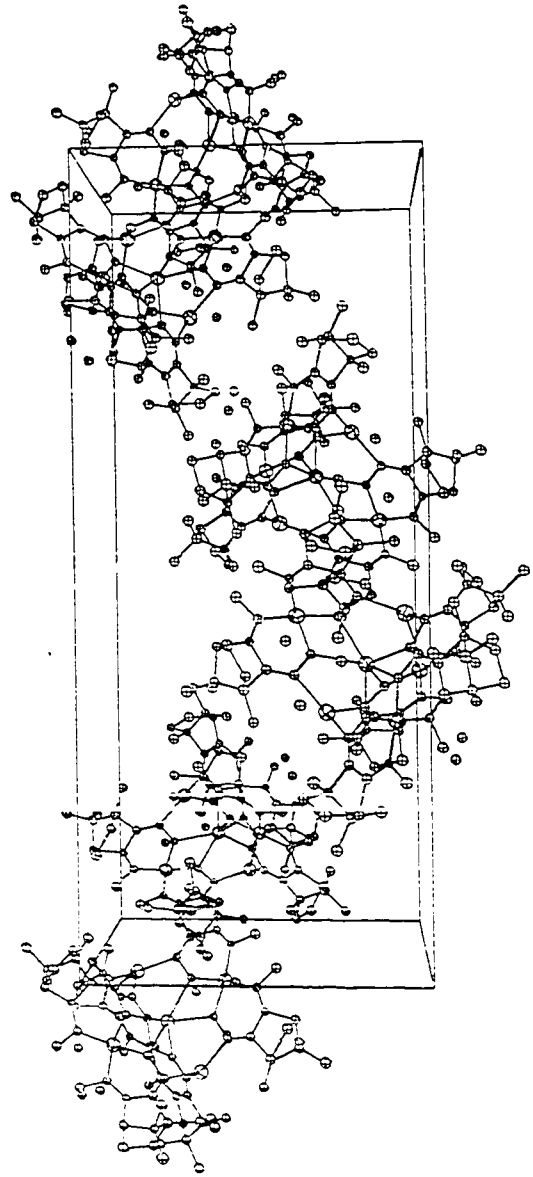

core for the molecule. The Ag1-Ag2-Ag3 angle is 178.1(2)°. The short silver-silver distances, Ag1-Ag2 3.059(5)Å and Ag2-Ag3 3.052(5)Å, suggest some metal-metal interactions. The Ag-Ag distance in metallic silver is 2.89Å(46).

Although there are no other bonding interactions between the nickel or silver atoms, these metals form an interesting nearly trigonal bipyramidal arrangement. The angle between the Ag1-Ag2-Ag3 line and the Ni1-Ni2-Ni3 least squares plane is 89.7°. The nickels are distorted from three-fold symmetry, Ni1-Ag2-Ni2 130.3(2)°, Ni1-Ag2-Ni3 103.2(2)°, and Ni2-Ag2-Ni3 126.5(2)°.

In each hexanuclear molecule, the linear chain of silver atoms is parallel to the ligand coordination planes of each $Ni(\delta\text{-HCQD})_2^-$ group. The Ag2 atom is coordinated to the O1 and O4 oxime oxygens of each nickel group, forming three four-membered chelate rings. The average silver-oxygen bond length is 2.49(3)Å, well within the range of Ag-O bonds (2.15-2.88Å) reported in the literature (47-50). Only the nitrogen atoms N1 and N4 coordinate to Ag1 and Ag3. This type of coordination gives the outer silver atoms a trigonal pyramidal configuration. The average silver-nitrogen bond length is 2.20(4)Å, comparable to other Ag-N bonds (2.11-2.51Å) reported in the literature (48-52). The distance of Ag1 and Ag3 from the least squares planes defined by

1N4-2N4-3N4 and 1N1-2N1-3N1, respectively, are both 0.52Å.

Although the molecular structure of the Ni(δ-HCQD)$_2$ complex, a reactant in the preparation of this cluster complex, has been described as having a trans configuration of δ-HCQD$^-$ ligands (6), the structure of the hexanuclear molecule reveals a cis configuration around each nickel atom. The average nickel-nitrogen distance of 1.86(4)Å is comparable to the average 1.855(4)Å found in the Ni (δ-HCQD)$_2$ complex (6). However, the average nickel-oxygen distance of 1.87(3)Å is considerably larger than 1.830(4)Å found for Ni(δ-HCQD)$_2$ (6). This lengthening is presumably due to the coordination of Ag2 to these oxygens. The silver-oxygen coordination and the cis configuration of ligands affect the bond angles around the nickels. The O1-Ni-O4 angles (75.9(1), 77.2(1) and 80.5(1)°) are consistently smaller than their counterparts (both greater than 85°) in the three nickel anion groups. The nickels deviate from least squares planes composed of Ni-O1-O4-N2-N3 by only 0.04, 0.006, and 0.01Å for the three groups. The average C-C (1.53Å), C=N (1.28Å), and N-O (1.38Å) distances in the ligands correspond well with those found in the structure of Ni(δ-HCQD)$_2$ (6).

The band in the infrared spectrum occurring at 1615 cm$^{-1}$ is most likely the ν (C=N) frequency of the oxime groups

coordinated to both silver and nickel atoms. The other $\nu$ (C=N) absorption, which probably arises from the oximes which are nitrogen coordinated to the nickels, remains unchanged at 1560 $cm^{-1}$, as previously reported for $Ni(\delta\text{-HCQD})_2$ (5).

The cis configuration of ligands imposes interesting constraints upon the intramolecular hydrogen bonds. This configuration forms six-membered, hydrogen-bonded, chelate rings. The 02-03 distances (2.38(5), 2.40(5), and 2.27(4)Å) are shorter than the 2.40Å distance reported for the dimethylglyoximato complex $Ni(HDMG)_2$ (45). The average N2-02-03 and N3-03-02 angles are 99.4° and 98.7°, respectively.

The hexanuclear molecules tend to pair up through van der Waals type interactions between molecules along the two fold screw axes parallel to the c axis. There are also two sites for $CHCl_3$ molecules near each hexanuclear molecule; however, the distances between the cluster molecules and the solvent sites (greater than 3.4Å) indicate only weak van der Waals type interactions. No evidence for intermolecular hydrogen bonding was found.

# SECTION V. THE CRYSTAL AND MOLECULAR STRUCTURE OF CIS-DICHLOROBIS(METHYLDIPHENYLPHOSPHINITE)-PALLADIUM(II)

## Introduction

Palladium(II) forms square planar complexes of the type $L_2MX_2$ where X represents a monodentate uninegative anion and L a monodentate ligand with a lone pair of electrons. These complexes have received considerable attention because they serve as model systems for square planar substitution and isomerization reactions and because these reactions proceed at rates which are conveniently measured by conventional techniques (53). Complexes of sterically hindered phosphines have been found to undergo reactions which, as a class, may be termed "internal-, cyclo-, or ortho-metallation reactions" (53). Many of these complexes, which undergo internal metallations, are very good catalysts for selective hydrogenation of unsaturated organic substrates (9). Recently, these complexes have been found to catalyze a number of reactions including alcohol carbonylation (10) and the stereocontrolled introduction of an acyclic unit onto cyclic organic systems (e.g., steroids) (54). The complex cis-dichlorobis-(methyldiphenylphosphinite)-palladium(II), $PdCl_2[P(OMe)Ph_2]_2$, has been shown to

catalyze the carboxylation of certain olefins (11). A single crystal x-ray study was undertaken to determine the structure of this complex.

## Experimental

The palladium complex was recrystallized from a saturated solution of 1:1 chloroform and carbon tetrachloride. A yellow crystal of approximate dimensions 0.1 x 0.1 x 0.2 mm was chosen for data collection. From four preliminary $\omega$ oscillation photographs taken at various $\chi$ and $\phi$ settings, nine independent reflections were selected, and their coordinates were input to an automatic indexing algorithm (13). The resulting reduced cell and reduced cell scalars indicated monoclinic symmetry. Axial oscillation photographs confirmed the mirror symmetry normal to the $\underline{b}$ axis. Observed layer line spacings were within experimental error of those predicted for this cell. The lattice constants, $\underline{a}$ = 12.539(6), $\underline{b}$ = 13.741(4), $\underline{c}$ = 15.147(4)Å, and $\beta$ = 94.65(4)° were determined from a least squares fit (14) to 12 strong, precisely-measured ($\pm 2\theta$) reflections at 25°C using graphite-monochromated Mo $K_\alpha$ radiation ($\lambda$=0.70954Å).

Intensity data were collected at 25°C using an automated, four-circle diffractometer designed and built

in this laboratory (15). Graphite-monochromated Mo $K_\alpha$ radiation was used for the data collection. All data (5053 reflections) within a $2\theta$ sphere of $50^\circ$ were measured in the hkl and $hk\bar{l}$ octants using an $\omega$-stepscan technique.

As a general check on electronic and crystal stability, the intensities of six standard reflections were remeasured every seventy-five reflections. Only one of these six standard reflections decreased substantially during the data collection period. Since the intensities of the remaining five reflections remained nearly constant throughout the data collection period, no decay correction was applied to the data. The data were corrected for Lorentz and polarization effects. No absorption correction was applied because the linear absorption coefficient was $\mu = 10.5\ cm^{-1}$ and the transmittance was $T = 0.84 \pm 0.06$. The estimated variance in each reflection was calculated by:

$$\sigma_I^2 = C_T + 2C_B + (0.03\ C_T)^2 + (0.03\ C_B)^2$$

where $C_T$ and $C_B$ are the total and background counts, and the factor 0.03 is an estimate of nonstatistical errors. The estimated standard deviation in each structure factor was determined by the finite difference method (16). The observed data ($I > 3\sigma_I$) were averaged yielding 2150 independent observed reflections. The systematic absence

of reflections with 0k0, k≠2n and h0l, h+l≠2n uniquely determined the space group to be $P_{2_1/n}$.

## Solution and Refinement

The coordinates of the palladium, phosphorous, and chlorine atoms were readily located on a three-dimensional Patterson map (31). The remaining nonhydrogen atoms were determined from subsequent structure factor (17) and electron density map calculations (31). Block matrix least squares refinement (17) of the positional and thermal parameters yielded a conventional residual $R = 0.113$ and a weighted residual $R_\omega = 0.138$. All but three of the nonhydrogen atoms were refined anisotropically. Hydrogen atom positions were calculated assuming 1.07Å bond distances and tetrahedral geometries for the methyl hydrogen. The hydrogens were included in subsequent refinements, but their positional and thermal parameters were not varied. Refinement cycles were carried out until the shifts in the positional parameters of the nonhydrogen atoms were less than 0.1 of the corresponding estimated errors. The hydrogen positions were recalculated after each set of cycles. Finally three cycles of full matrix least squares refinement (17) were carried out. The final conventional residual was $R = 0.108$ and weighted residual $R_\omega = 0.135$.

The function minimized was $\Sigma \omega||F_o| - |F_c||^2$ with weights $\omega = 1/\sigma_F{}^2$. The scattering factors for the nonhydrogen atoms were those of Hanson et al., (18) corrected for anomalous dispersion effects (19). The hydrogen scattering factors were those of Stewart et al., (43). The final structural parameters are listed in Table 9. Selected bond distances and angles are presented in Table 10. Stereoscopic views (44) of molecule and the unit cell are illustrated in Figures 9 and 10, respectively.

## Discussion

The complex has approximately cis square-planar geometry around the palladium. However, there are small but significant distortions from this geometry since both the Cl1-Pd-Cl2 and P1-Pd-P2 bond angles have opened about 2° and 7°, respectively, from their theoretical value of 90°. The chlorine and phosphorus atoms are distorted (± 0.14 to ± 0.15Å) from a least squares plane of these atoms, with P1 and Cl1 shifted to one side of the plane and P2 and Cl2 shifted to the other side of the plane.

The palladium-phosphorus bonds in this compound (Pd-P1 2.230(7)Å and Pd-P2 2.244(6)Å) are shorter than those found in cis-$PdCl_2(PMe_2Ph)_2$, Pd-P 2.260(2)Å, (55)

Table 9. Final structural parameters for $PdCl_2[P(OMe)Ph_2]_2$

(a) Final positional parameters

| Atom | x | y | z |
|---|---|---|---|
| Pd | -0.0748(2) | 0.1592(1) | 0.1637(1) |
| Cl1 | 0.1096(6) | 0.1269(5) | 0.1701(4) |
| Cl2 | -0.1052(6) | 0.0293(4) | 0.2602(4) |
| P1 | -0.2531(5) | 0.1617(5) | 0.1458(3) |
| P2 | -0.0458(6) | 0.2918(4) | 0.0826(4) |
| O1 | -0.3119(13) | 0.1769(11) | 0.2333(9) |
| O2 | -0.1310(16) | 0.3790(11) | 0.0809(10) |
| C1A | -0.3109(23) | 0.0435(16) | 0.1034(13) |
| C2A | -0.4051(29) | 0.0150(20) | 0.1235(15) |
| C3A | -0.4516(18) | -0.0701(15) | 0.0883(12) |
| C4A | -0.3913(34) | -0.1250(21) | 0.0338(18) |
| C5A | -0.2910(33) | -0.0982(22) | 0.0132(18) |
| C6A | -0.2451(20) | -0.0116(19) | 0.0521(17) |
| C7A | -0.2655(28) | 0.2285(22) | 0.3098(15) |
| C1B | -0.3238(18) | 0.2424(14) | 0.0670(12) |
| C2B | -0.3913(19) | 0.3139(16) | 0.0938(14) |
| C3B | -0.4457(22) | 0.3744(18) | 0.0329(22) |
| C4B | -0.4380(31) | 0.3614(19) | -0.0559(22) |
| C5B | -0.3702(27) | 0.2916(24) | -0.0841(17) |
| C6B | -0.3159(22) | 0.2306(18) | -0.0238(15) |
| C1C | 0.0773(18) | 0.3509(14) | 0.1114(14) |
| C2C | 0.1548(20) | 0.3806(15) | 0.0526(12) |
| C3C | 0.2471(27) | 0.4306(24) | 0.0754(20) |
| C4C | 0.2684(24) | 0.4534(19) | 0.1626(20) |
| C5C | 0.1985(21) | 0.4274(20) | 0.2244(17) |
| C6C | 0.1096(22) | 0.3747(16) | 0.2015(16) |
| C7C | -0.1491(22) | 0.4385(19) | 0.1502(18) |

Table 9. Continued

| Atom | x | y | z |
|---|---|---|---|
| C1D | -0.0477(20) | 0.2689(16) | -0.0346(12) |
| C2D | -0.0285(24) | 0.1764(18) | -0.0640(16) |
| C3D | -0.0451(28) | 0.1554(21) | -0.1558(19) |
| C4D | -0.0710(28) | 0.2283(27) | -0.2149(17) |
| C5D | -0.0988(27) | 0.3152(22) | -0.1848(15) |
| C6D | -0.0822(26) | 0.3381(17) | -0.0971(15) |

Table 9. Continued

(b) Final thermal parameters[a]

| Atom | $\beta_{11}$ | $\beta_{22}$ | $\beta_{33}$ | $\beta_{12}$ | $\beta_{13}$ | $\beta_{23}$ |
|---|---|---|---|---|---|---|
| Pd | 82(2) | 54(1) | 37(1) | - 4(1) | 0(1) | 2(1) |
| U1 | 78(6) | 78(5) | 76(4) | -15(4) | 10(4) | 11(3) |
| U2 | 96(7) | 65(4) | 51(3) | - 7(4) | 2(3) | 18(3) |
| P1 | 64(5) | 64(4) | 34(2) | 9(4) | 4(2) | 0(3) |
| P2 | 88(7) | 44(3) | 40(2) | - 3(4) | 0(3) | 0(2) |
| O1 | 75(15) | 83(11) | 41(7) | - 5(11) | 13(8) | - 6(7) |
| O2 | 118(21) | 50(10) | 71(9) | 14(12) | - 8(10) | -16(8) |
| C1A | 94(26) | 51(14) | 41(10) | 0(16) | 10(12) | 15(9) |
| C2A | 182(41) | 79(21) | 42(12) | 6(24) | 9(17) | 15(13) |
| C3A | 5.6(4) | | | | | |
| C4A | 167(43) | 71(20) | 60(14) | -32(25) | -24(20) | 10(13) |
| C5A | 176(48) | 68(21) | 60(15) | 5(26) | -12(20) | -13(14) |
| C6A | 46(22) | 78(19) | 78(15) | 28(17) | 10(14) | 2(14) |
| C7A | 186(44) | 113(25) | 44(12) | - 9(25) | 11(17) | -25(14) |
| C1B | 3.3(4) | | | | | |
| C2B | 52(20) | 52(15) | 61(12) | -10(14) | - 4(12) | 0(10) |
| C3B | 82(27) | 51(16) | 118(23) | 41(16) | -23(19) | - 4(15) |
| C4B | 157(41) | 46(18) | 86(19) | 10(21) | -55(21) | 10(14) |

[a]The anisotropic thermal parameters are defined by $T = \exp -(h^2\beta_{11} + k^2\beta_{22} + l^2\beta_{33} + 2hk\beta_{12} + 2hl\beta_{13} + 2kl\beta_{23})$ . The thermal parameters for C3A, C1B, and C2C are isotropic B values.

Table 9. Continued

| Atom | $\beta_{11}$ | $\beta_{22}$ | $\beta_{33}$ | $\beta_{12}$ | $\beta_{13}$ | $\beta_{23}$ |
|---|---|---|---|---|---|---|
| C5B | 110(34) | 90(22) | 64(15) | -53(23) | -36(17) | 18(15) |
| C6B | 83(27) | 72(17) | 56(12) | 2(17) | - 1(13) | - 4(12) |
| C1C | 62(20) | 41(13) | 54(11) | -27(14) | - 6(11) | - 6(10) |
| C2C | 4.8(4) | | | | | |
| C3C | 119(34) | 98(27) | 87(19) | -14(24) | 18(19) | - 4(18) |
| C4C | 83(29) | 83(19) | 87(18) | 47(20) | -11(18) | - 2(15) |
| C5C | 33(23) | 99(21) | 73(15) | -16(18) | - 4(14) | 11(14) |
| C6C | 89(26) | 64(15) | 70(14) | -61(17) | -30(15) | 19(12) |
| C7C | 81(28) | 72(19) | 89(17) | 50(19) | 0(16) | -19(15) |
| C1D | 74(24) | 54(14) | 39(10) | -13(15) | -12(11) | - 8(10) |
| C2D | 118(30) | 68(18) | 63(13) | 42(20) | 34(15) | 12(12) |
| C3D | 149(37) | 85(21) | 68(16) | 18(24) | 16(18) | -38(16) |
| C4D | 118(36) | 132(29) | 52(14) | -25(26) | 13(16) | -10(17) |
| C5D | 156(38) | 87(22) | 41(12) | 4(23) | - 4(15) | 3(13) |
| C6D | 198(41) | 45(14) | 48(12) | 16(21) | 28(16) | - 4(12) |

Table 10. Bond distances (Å) and angles (°) for $PdCl_2$ $[P(OMe)Ph_2]_2$

(a) Bond distances

| | | | | | |
|---|---|---|---|---|---|
| Pd | - Cl1 | 2.349(8) | Pd | - Cl2 | 2.358(6) |
| Pd | - P1 | 2.230(7) | Pd | - P2 | 2.244(6) |
| P1 | - O1 | 1.582(16) | P2 | - O2 | 1.604(19) |
| P1 | - C1A | 1.871(24) | P2 | - C1C | 1.767(23) |
| P1 | - C1B | 1.808(20) | P2 | - C1D | 1.801(19) |
| O1 | - C7A | 1.440(30) | O2 | - C7C | 1.364(31) |
| C1A | - C2A | 1.304(45) | C1C | - C2C | 1.430(32) |
| C1A | - C6A | 1.401(36) | C1C | - C6C | 1.430(32) |
| C2A | - C3A | 1.393(35) | C2C | - C3C | 1.366(40) |
| C3A | - C4A | 1.387(40) | C3C | - C4C | 1.363(42) |
| C4A | - C5A | 1.370(58) | C4C | - C5C | 1.380(41) |
| C5A | - C6A | 1.428(40) | C5C | - C6C | 1.351(37) |
| C1B | - C2B | 1.379(31) | C1D | - C2D | 1.374(33) |
| C1B | - C6B | 1.396(30) | C1D | - C6D | 1.386(31) |
| C2B | - C3B | 1.380(36) | C2D | - C3D | 1.419(37) |
| C3B | - C4B | 1.368(47) | C3D | - C4D | 1.365(43) |
| C4B | - C5B | 1.373(47) | C4D | - C5D | 1.334(47) |
| C5B | - C6B | 1.378(38) | C5D | - C6D | 1.365(32) |

(b) Bond angles

| | | | | | | | | |
|---|---|---|---|---|---|---|---|---|
| Cl1 | - Pd | - Cl2 | 92.3(2) | Cl1 | - Pd | - P2 | 88.5(3) |
| P1 | - Pd | - P2 | 97.3(3) | Cl2 | - Pd | - P1 | 82.9(2) |
| Pd | - P1 | - O1 | 115.5(6) | Pd | - P2 | - O2 | 118.6(7) |
| Pd | - P1 | - C1A | 112.6(9) | Pd | - P2 | - C1C | 114.5(7) |
| Pd | - P1 | - C1B | 121.5(8) | Pd | - P2 | - C1D | 114.1(8) |
| P1 | - O1 | - C7A | 123.6(17) | P2 | - O2 | - C7C | 126.0(16) |
| O1 | - P1 | - C1A | 102.0(10) | O2 | - P2 | - C1C | 103.2(10) |
| O1 | - P1 | - C1B | 103.6(9) | O2 | - P2 | - C1D | 99.2(10) |
| C1A | - P1 | - C1B | 98.6(10) | C1C | - P2 | - C1D | 105.4(11) |
| P1 | - C1A | - C2A | 120.9(19) | P2 | - C1C | - C2C | 127.0(16) |
| P1 | - C1A | - C6A | 115.5(20) | P2 | - C1C | - C6C | 121.0(18) |
| P1 | - C1B | - C2B | 121.5(15) | P2 | - C1D | - C2D | 119.5(16) |
| P1 | - C1B | - C6B | 120.6(17) | P2 | - C1D | - C6D | 122.1(17) |
| C6A | - C1A | - C2A | 123.6(23) | C6C | - C1C | - C2C | 112.0(20) |
| C1A | - C2A | - C3A | 121.4(25) | C1C | - C2C | - C3C | 126.2(20) |

Table 10. Continued

| | | | |
|---|---|---|---|
| C2A - C3A - C4A | 116.9(26) | C2C - C3C - C4C | 117.1(28) |
| C3A - C4A - C5A | 123.0(27) | C3C - C4C - C5C | 120.8(27) |
| C4A - C5A - C6A | 118.5(28) | C4C - C5C - C6C | 121.4(25) |
| C5A - C6A - C1A | 116.3(26) | C5C - C6C - C1C | 122.1(24) |
| C6B - C1B - C2B | 117.8(19) | C6D - C1D - C2D | 117.8(19) |
| C1B - C2B - C3B | 120.9(22) | C1D - C2D - C3D | 119.3(22) |
| C2B - C3B - C4B | 120.5(26) | C2D - C3D - C4D | 120.1(26) |
| C3B - C4B - C5B | 119.5(28) | C3D - C4D - C5D | 119.2(25) |
| C4B - C5B - C6B | 120.3(26) | C4D - C5D - C6D | 121.0(26) |
| C5B - C6B - C1B | 120.8(24) | C5D - C6D - C1D | 121.4(23) |

Table 11. Least squares planes[a] for $PdCl_2$ $[P(OMe)Ph_2]_2$

| Atom | D[b] | Atom | D |
|---|---|---|---|
| | Plane 1: Cl1-Cl2-P1-P2<br>-0.0001x + 0.5954y + 0.8034z = 3.2446 | | |
| Pd | 0.044 | P1 | -0.153 |
| Cl1 | -0.143 | P2 | 0.145 |
| Cl2 | 0.151 | | |
| | Plane 2: C1A-C2A-C3A-C4A-C5A-C6A<br>-0.3293x + 0.5052y - 0.7977z = 0.3532 | | |
| C1A | 0.029 | C4A | 0.002 |
| C2A | -0.014 | C5A | 0.013 |
| C3A | -0.002 | C6A | -0.028 |
| | Plane 3: C1B-C2B-C3B-C4B-C5B-C6B<br>-0.7629x - 0.6443y - 0.0544z = 0.9664 | | |
| C1B | -0.007 | C4B | 0.018 |
| C2B | 0.008 | C5B | -0.016 |
| C3B | -0.014 | C6B | 0.011 |
| | Plane 4: C1C-C2C-C3C-C4C-C5C-C6C<br>-0.4838x + 0.8636y - 0.1418z = 3.5006 | | |
| C1C | 0.022 | C4C | 0.0 |
| C2C | -0.005 | C5C | 0.020 |
| C3C | -0.006 | C6C | -0.031 |

[a]Planes are defined as $C_1x + C_2y + C_3z - C_4$ where x, y, and z are Cartesian coordinates.

[b]D represents the distance (Å) of the given atom from the plane.

Table 11. Continued

| Atom | D[b] | Atom | D |
|---|---|---|---|
| Plane 5: C1D-C2D-C3D-C4D-C5D-C6D<br>0.9620x + 0.2564y - 0.0941z = 0.4456 | | | |
| C1D | 0.016 | C4D | 0.061 |
| C2D | -0.001 | C5D | -0.046 |
| C3D | -0.037 | C6D | 0.007 |

Figure 9. A stereoscopic view of $PdCl_2[P(OMe)Ph_2]_2$. The thermal ellipsoids are drawn at the 50% probability level.

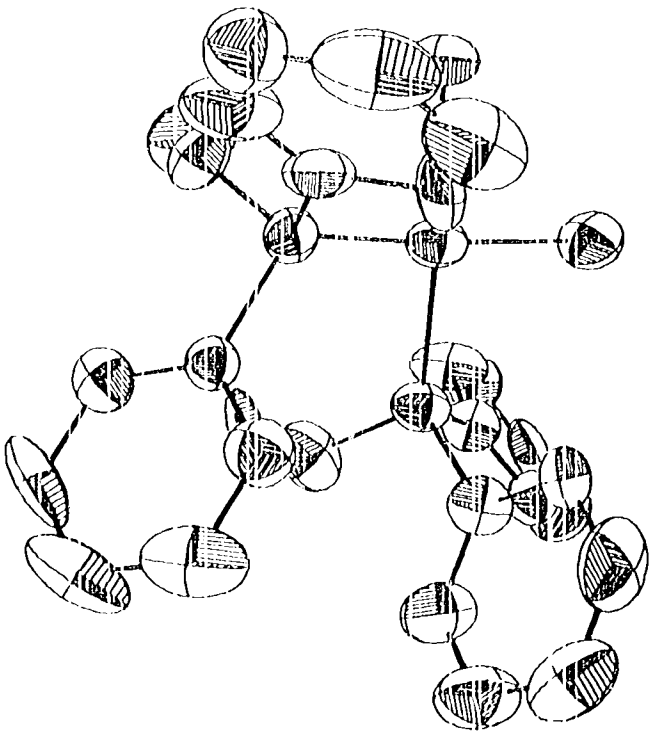

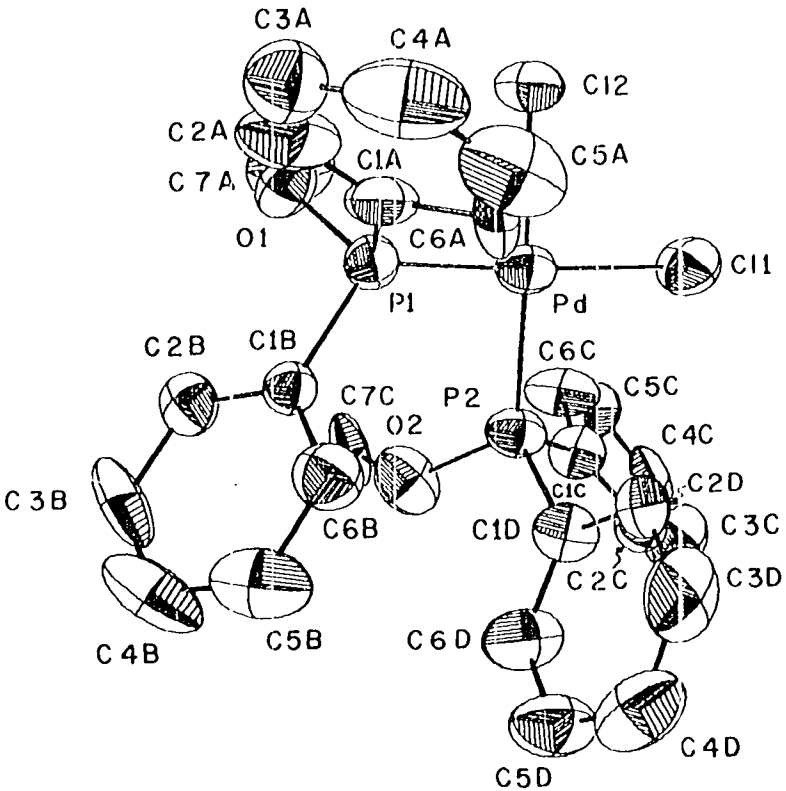
C3A
C4A
C12
C2A
C5A
C7A
C1A
O1
C6A
C11
P1
Pd
C2B
C1B
C6C
C7C
P2
C5C
O2
C4C
C3B
C2D
C1C
C1D
C3C
C6B
C2C
C3D
C4B
C5B
C6D
C4D
C5D

Figure 10. A stereoscopic view of the unit cell of $PdCl_2[P(OMe)Ph_2]_2$ projected along the b axis.

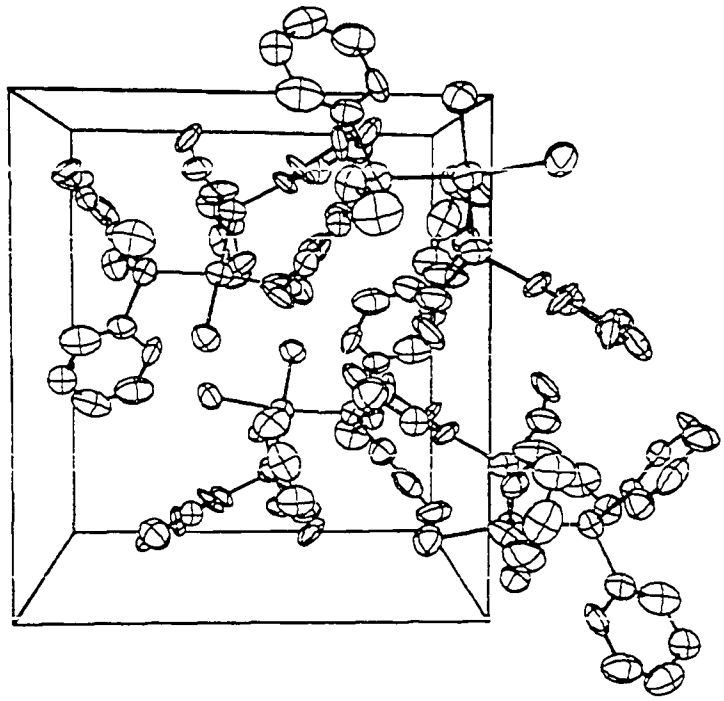

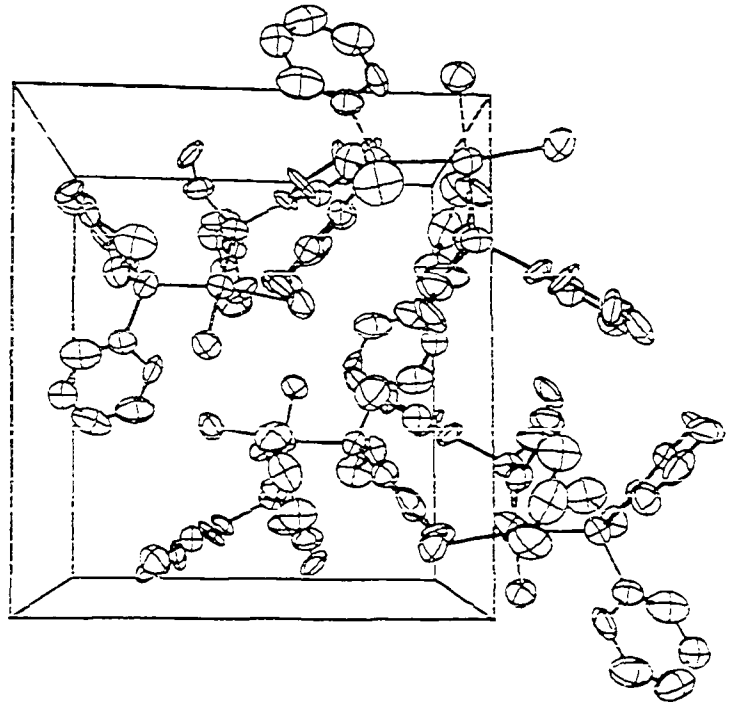

and trans-$PdI_2(PMe_2Ph)_2$, Pd-P 2.333(7)Å (56). Also the palladium-chlorine bonds (Pd-Cl1 2.349(8)Å and Pd-Cl2 2.358(6)Å) are longer than those found in cis-$PdCl_2(PMe_2Ph)_2$, Pd-Cl 2.362(3)Å (55) and trans-$PdCl_2(DMSO)_2$, Pd-Cl 2.287(2)Å (57). These results generally agree with those expected from a strong "trans effect." That is, the bond trans to a strongly "trans-directing" ligand, such as phosphorus, is weaker and therefore longer than a bond trans to the less "trans-directing" chlorine. These results also confirm the fact that phosphinite ligands exert a stronger trans effect than do phosphine ligands.

The phenyl rings of the two phosphinite ligands pack so as to minimize repulsions between the ligands. There are no carbon-carbon interactions between the two ligands of less than 3.42Å. Phenyl ring B on phosphorus P1 and phenyl ring D on phosphorus P2 are partially aligned with an interplanar angle of 26.6°.

The opening of the Cl1-Pd-Cl2 angle was unexpected. In the compound cis-$PdCl_2(PMe_2Ph)_2$, (53) the phosphorus ligands pack so as to compress the Cl-Pd-Cl angle. Although there are no intermolecular hydrogen bonding interactions, there are a number of distances between the chlorines and the carbons (Cl1-C6C 3.44(2)Å, Cl2-C6A 3.52(2)Å, and Cl2-C7A 3.51(3)Å) which are less than the

sum of the van der Waals radii (34). Perhaps these interactions and the weakened Pd-Cl bonds permit the Cl1-Pd-Cl2 angle to open.

The carbon atoms in the phenyl rings show no significant deviations from the corresponding least squares planes (see Table 11). The average bond angles in the four phenyl rings are 119.9°, 120.0°, 119.9°, and 119.8°, in good agreement with the expected value of 120°. The average bond distances in the four rings, 1.380, 1.379, 1.387, and 1.374Å, are all a bit shorter than the expected value of 1.396Å (34). These results and the apparently large thermal motion as illustrated by the carbon thermal ellipsoids suggest that the ligands may be librating.

The crystal packing forces are entirely of the van der Waals type. The closest palladium-palladium distance is 6.98Å, far too long for metal-metal interactions.

## SUMMARY

The single crystal x-ray characterizations of five inorganic compounds with novel bonding features were described. The metal atoms of $Lu_3S_4$ form periodic occupation waves throughout the primarily rock-salt structure. The metal atoms in 3-R $Nb_{1.06}S_2$ present two interesting points; the principal metal site is not completely occupied, and the metal in the van der Waals site is distorted from octahedral coordination by displacement along the three-fold axis. The structure of bis(δ-camphorquinonedioximato)nickel(II), $Ni(\delta\text{-HCQD})_2$, is the first reported structure in which the vic-dioxime ligands coordinate to the metal via nitrogen and oxygen donor atoms. A novel hexanuclear cluster complex, with three silver atoms forming a linear backbone, is the structurally characterized reaction product of $Ni(\delta\text{-HCQD})_2$ and $AgNO_3$. The structure of cis-dichlorobis(methyldiphenylphosphinite)palladium(II) is the first reported square-planar palladium complex in which phosphinite ligands are bonded cis to the metal.

## REFERENCES


1. Franzen, H. F.; Hariharan, A. V. J. Chem. Phys., 1979, 70, 4907.

2. Yoffe, A. D. Chem. Soc. Rev., 1976, 5, 51.

3. Murphy, D. W.; Trumbore, F. A. J. Crystal Growth, 1977, 39, 185.

4. Whittingham, M. S. J. Solid State Chem., 1979, 29, 303.

5. Nakamura, A.; Konishi, A.; Otsuka, S. J. Chem. Soc., Dalton Trans., 1979, 488.

6. Ma, M. S.; Angelici, R. J.; Powell, D.; Jacobson, R. A. J. Am. Chem. Soc., 1978, 100, 7068.

7. Bigotto, A.; Costa, G.; Glasso, V.; DeAlti, G. Spectrochim. Acta, 1970, A26, 1939.

8. Ma, M.S.; Angelici, R. J.; Powell, D.; Jacobson, R. A. submitted for publication to Inorg. Chem.

9. Bruner, H.; Bailar, J. C. Inorg. Chem., 1977, 12, 1465.

10. Rivetti, F.; Romano, U. J. Organomet. Chem., 1978, 154, 323.

11. Mrowca, J. J. U. S. Patent 3 906 015, 1975; Chem. Abstr., 1976, 84, 4507c.

12. Dismukes, J. P.; White, J. G. Inorg. Chem., 1964, 3, 1220.

13. Jacobson, R. A. J. Appl. Crystallogr., 1976, 9, 115.

14. Takusagawa, F. Department of Chemistry, Iowa State University, Ames, Iowa, private communication, 1975.

15. Rohrbaugh, W. J.; Jacobson, R. A. Inorg. Chem., 1974, 13, 2535.

16. Lawton, S. L.; Jacobson, R. A. Inorg. Chem., 1968, 1, 2124.

17. Lapp, R. L.; Jacobson, R. A. Ames, Iowa, Aug., 1979, DOE Report IS-4708.

18. Hanson, H. P.; Herman, F.; Lea, J. D.; Skillman, S. Acta Crystallogr., 1960, 17, 1040.

19. Templeton, D. H. In "International Tables for X-Ray Crystallography," MacGillavry, C. H.; Riek, G. D.; Lonsdale, K., ed.; Kynoch Press: Birmingham, England, 1962, Vol. III, Table 3.3.2.C.

20. Wiegers, G. A.; Jellinek, F. J. Solid State Chem., 1970, 1, 519.

21. Franzen, H. F.; Hariharan, A. V. J. Solid State Chem., 1978, 26, 189.

22. Range, K. T.; Leeb, R. Z. Naturforsch., 1975, B30, 637.

23. Whittingham, M. S.; Gamble, F. R. Mater. Res. Bull., 1975, 10, 363.

24. Morosin, B. Acta Crystallogr., 1974, B30, 551.

25. (a) Jellinek, F.; Brauer, G.; Muller, H. Nature, 1960, 185, 376.
(b) Kadijk, F.; Jellinek, F. J. Less-Common Metals, 1969, 19, 421.

26. Fisher, W. G.; Sienko, M. Inorg. Chem., 1980, 19, 39.

27. Thompson, A. H. Phys. Rev. Lett., 1975, 34, 520.

28. Boswell, F. W.; Prodan, A.; Corbett, J. M. Phys. Status Solidi, 1976, (a) 35, 591.

29. DeMeulenaer, J.; Tompa, H. Acta Crystallogr., 1965, 19, 1014.

30. Busing, W. R.; Martin, K. O.; Levy, H. A. Oak Ridge, Tennessee, Nov., 1965, AEC Report ORNL-TM-305.

31. Hubbard, C. R.; Quicksall, C. O.; Jacobson, R. A. Ames, Iowa, June, 1971, AEC Report IS-2625.

32. Thomas, L. H.; Umeda, K. J. Chem. Phys., 1956, 26, 293.

33. Tomiie, Y.; Stam, C. H. Acta Crystallogr., 1958, 11, 126.

34. Pauling, L. "The Nature of the Chemical Bond," 3rd ed.; Cornell University Press: Ithaca, New York, 1960, p 98, p 233.

35. Gamble, F. R. J. Solid State Chem., 1974, 9, 358.

36. Chakravorty, A. Coord. Chem. Rev., 1974, 13, 1.

37. O'Connor, M. J. Progress Inorg. Chem., 1971, 14, 277.

38. Perrin, D. D. "Organic Complexing Reagents," Interscience Publishers: New York, New York, 1964.

39. (a) Schrauzer, G. N. Accounts Chem. Res., 1968, 1, 97.
(b) Schrauzer, G. N. Angew. Chem., Int. Edit. Eng., 1976, 15, 417.

40. Ohgo, Y.; Natori, Y.; Takeuchi, S.; Yoshimura, J. Chem. Lett., 1974, 11, 1327.

41. (a) Rechani, P. R.; Nakon, R.; Angelici, R. J. Bioinorg. Chem., 1976, 5, 329.
(b) Bedell, S. A.; Rechani, P. R.; Angelici, R. J.; Nakon, R. Inorg. Chem., 1977, 16, 972.

42. Nakamura, A.; Konishi, A.; Tatsuno, Y.; Otsuka, S. J. Am. Chem. Soc., 1978, 100, 3443.

43. Stewart, R. F.; Davidson, E. R.; Simpson, W. T. J. Chem. Phys., 1965, 42, 3175.

44. Johnson, C. K. Oak Ridge, Tennessee, March, 1971, AEC Report ORNL-3794 (Second Revision).

45. (a) Grodycki, L. E.; Rundle, R. E. Acta Crystallogr., 1953, 6, 487.
(b) Williams, D. E.; Wohlauer, G.; Rundle, R. E. J. Am. Chem. Soc., 1959, 81, 755.

46. Pearson, W. B. "A Handbook of Lattice Spacings, Structures of Metals and Alloys," 2nd ed.; Permagon Press: Oxford, England, 1967.

47. Hunt, G. W.; Lee, T. C.; Amma, E. L. Inorg. Nucl. Chem. Lett., 1974, 10, 909.

48. Delourne, P. J. P.; Loiseleur, R. F. H. Acta Crystallogr., 1977, B33, 2709.

49. Kuyper, J.; Vrieze, K.; Olie, K. Crystal Struct. Comm., 1976, 5, 179.

50. Palgaard, G. A. P.; Hazell, A. C.; Hazell, R. G. Acta Crystallogr., 1974, B30, 2721.

51. Britton, D.; Chow, Y. M. Acta Crystallogr., 1977, B33, 697.

52. Bigoli, F.; Laporti, E.; Pellinghelli, M. A. Crystal Struct. Comm., 1975, 4, 127.

53. Verstuyft, A. W.; Redfield, D. A.; Cary, L. W.; Nelson, J. H. Inorg. Chem., 1977, 16, 2776, and references cited therein.

54. Trost, B. M.; Verhoeven, T. R. J. Am. Chem. Soc. 1978, 100, 3435.

55. Martin, L. L.; Jacobson, R. A. Inorg. Chem., 1971, 10, 1795.

56. Bailey, N. A.; Mason, R. J. Chem. Soc., 1968, 2594.

57. Bennett, M. J.; Cotton, F. A.; Weaver, D. L. Acta Crystallogr., 1967, 23, 788.

58. Powell, D. R.; Jacobson, R. A. Ames, Iowa, April, 1980, DOE Report IS-4737.

59. Rogers, J.; Jacobson, R. A. Ames, Iowa, July, 1969, AEC Report IS-2155.

60. Singleton, R. C. Comm. ACM, 1969, 12, 185.

61. Adapted from H20-0586-0/360 Scientific Subroutine Package (PL/1) Program Description and Operation Manual, International Business Machines, Inc., 1968.

62. Gentleman, W. M.; Sande, G. In Proceedings--Fall Joint Computer Conference, 1966, p. 563.

ACKNOWLEDGMENTS

The author is indebted to Professor Robert A. Jacobson for his patience and his inspiring guidance during the course of this work and to all members of the x-ray crystallography group whose assistance and friendship have helped make graduate school an enjoyable experience. The author wishes to thank Diane Kuhlers for typing this manuscript.

To his parents and family, the author extends his deepest gratitude and love.

# APPENDIX: FOUR, A GENERAL CRYSTALLOGRAPHIC FOURIER PROGRAM

## Introduction

Fourier transforms are valuable tools for both the solution and refinement of crystal structures. A report is available (58) which describes the operation and use of a program written in the FORTRAN programming language for the calculation of two- and three-dimensional, discrete Fourier transforms. The program has been designed to calculate a Fourier map for any space group. Much of the theoretical basis for this program is detailed in the report of an earlier Fourier program written by Rogers and Jacobson (59); however, the implementation in the current program is completely different. The newer program performs the section and line summations using regular Fourier methods. The final summation is carried out using a fast Fourier transform algorithm. (If the fast Fourier algorithm were to be used for the first two summations, much more storage would be needed and a large number of unnecessary calculations would have to be performed.)

A number of features have been included in this program which should facilitate its implementation. All

calculations are carried out in one program, reducing the chance of user input error. The output permits a great deal of flexibility. The map may be oriented in any of six orientations with grid sizes of 16, 32, 64, or 128. Printed maps may be in the form of two, three, or four digit number output, or two or three digit base 36 character output. Also Patterson maps can be automatically scaled by the computer, if desired. Maps are written to disk, one line at a time, as the integer representation of each line. The program was written in the FORTRAN programming language to simplify any changes necessary in the transfer of the program to other computer facilities. The next sections present a mathematical derivation and a detailed description of the program.

## General Description

The electron density at a particular point (x,y,z) may be written in the form:

$$\rho(x,y,z) = \frac{1}{V} \sum_{h=-\infty}^{\infty} \sum_{k=-\infty}^{\infty} \sum_{\ell=-\infty}^{\infty} F(hk\ell) \exp(-2\pi i \underline{h}^t \cdot \underline{r})$$

with $\underline{h}^t \cdot \underline{r} = (hx+ky+\ell z)$ and $F = A+iB$. Separating $F(hk\ell)$ into its Friedel-related components permits the summations over one of the indices, say $\ell$, to be carried out from 0 to $\infty$.

$$\rho(x,y,z) = \frac{1}{V} \sum_{-\infty}^{\infty}_{h} \sum_{-\infty}^{\infty}_{k} \sum_{0}^{\infty}_{\ell} (A+iB)\exp(-2\pi i\underline{h}^t\cdot\underline{r}) + \qquad (2)$$

$$(A-iB)\exp(-2\pi i(-\underline{h}^t\cdot\underline{r}))$$

Writing the exponentials in their trigonometric forms, equation (2) becomes

$$\rho(x,y,z) = \frac{1}{V} \sum_{-\infty}^{\infty}_{h} \sum_{-\infty}^{\infty}_{k} \sum_{0}^{\infty}_{\ell} (A+iB)\ (\cos 2\pi\underline{h}^t\cdot\underline{r} - i\sin 2\pi\underline{h}^t\cdot\underline{r})$$

$$+ (A-iB)\ (\cos 2\pi\underline{h}^t\cdot\underline{r} + i\sin 2\pi\underline{h}^t\cdot\underline{r}) \qquad (3)$$

$$\rho(x,y,z) = \frac{2}{V} \sum_{\infty}^{\infty}_{h} \sum_{\infty}^{\infty}_{k} \sum_{0}^{\infty}_{\ell} (A\cos 2\pi\underline{h}^t\cdot\underline{r} + B\sin 2\pi\underline{h}^t\cdot\underline{r}) \qquad (4)$$

Factoring the trigonometric terms speeds up the calculation. The results of the summation over one index are calculated for a given grid value. These results are recalled each time a summation over another index is calculated. Let $C_h = \cos 2\pi hx$, $S_h = \sin 2\pi hx$, etc.

$$\rho(x,y,z) = \frac{2}{V} \sum_{h=-\infty}^{\infty} \sum_{k=-\infty}^{\infty} \sum_{\ell=0}^{\infty} A(C_h C_{k,\ell} - S_h S_{k,\ell}) +$$

$$B(S_h C_{k,\ell} + C_h S_{k,\ell}) \qquad (5)$$

$$\rho(x,y,z) = \frac{2}{V} \sum_{h=\infty}^{\infty} \sum_{k=\infty}^{\infty} \sum_{\ell=0}^{\infty} A(C_h C_k C_\ell - C_h S_k S_\ell - S_h C_k S_\ell - S_h S_k C_\ell)$$

$$+ B(C_h C_k S_\ell + C_h S_k C_\ell + S_h C_k C_\ell - S_h S_k S_\ell) \qquad (6)$$

In this expression the trigonometric terms are similar for the coefficients $A(hk\ell)$, $A(\bar{h}k\ell)$, $A(h\bar{k}\ell)$, and $A(\bar{h}\bar{k}\ell)$, and likewise for B. Stating these terms explicitly rather than including them in the summation, and accounting for the even and odd nature of the cosine and sine functions yields equation (7).

$$(x,y,z) = \frac{2}{V} \sum_{0}^{\infty}_{h} \sum_{0}^{\infty}_{k} \sum_{0}^{\infty}_{\ell} \underline{/}\overline{A}(hk\ell)+A(\bar{h}\bar{k}\ell)+A(h\bar{k}\ell)+A(\bar{h}\bar{k}\ell)\underline{/}$$

$$C_h C_k C_\ell$$

$$+ \underline{/}\overline{-}A(hk\ell)-A(\bar{h}k\ell)+A(h\bar{k}\ell)+A(\bar{h}\bar{k}\ell)\underline{/}C_h S_k S$$

$$+ \underline{/}\overline{-}A(hk\ell)+A(\bar{h}k\ell)-A(h\bar{k}\ell)+A(\bar{h}\bar{k}\ell)\underline{/}S_h C_k S_\ell$$

$$+ \underline{/}\overline{-}A(hk\ell)+A(\bar{h}k\ell)+A(h\bar{k}\ell)-A(\bar{h}\bar{k}\ell)\underline{/}S_h S_k C_\ell \quad (7)$$

$$+ \underline{/}\overline{B}(hk\ell)+B(\bar{h}k\ell)+B(h\bar{k}\ell) + B(\bar{h}\bar{k}\ell)\underline{/}C_h C_k S_\ell$$

$$+ \underline{/}\overline{B}(hk\ell)+B(\bar{h}k\ell)-B(h\bar{k}\ell)-B(\bar{h}\bar{k}\ell)\underline{/}C_h S_k C_\ell$$

$$+ \underline{/}\overline{B}(hk\ell)-B(\bar{h}k\ell)+B(h\bar{k}\ell)-B(\bar{h}\bar{k}\ell)\underline{/}S_h C_k C_\ell$$

$$+ \underline{/}\overline{-}B(hk\ell)+B(\bar{h}k\ell)+B(h\bar{k}\ell)-B(\bar{h}\bar{k}\ell)\underline{/}S_h S_k S_\ell$$

This is only one of the possible choices of four data octants out of eight which can be chosen so that none of the four octants are Friedel related. The appropriate signs for the A and B terms of all octants are compactly stored in an 8 x 8 array.

If the sum of the four structure factor terms in equation (7) are labeled $A_1$, $A_2$, $A_3$, $A_4$, $B_1$, $B_2$, $B_3$, and $B_4$, respectively, then it is possible to factor equation (7) as follows:

$$\rho(x,y,z) = \frac{2}{V} \sum_{0}^{h=\infty} \sum_{0}^{k=\infty} \{ \underline{/}\overline{\sum_{0}^{\ell=\infty}}(A_1 C_\ell + B_1 S_\ell) \overline{/} C_h C_k$$

$$+ \underline{/}\overline{\sum_{0}^{\ell}}(A_2 S_\ell + B_2 C_\ell) \overline{/} C_h S_k$$

$$+ \underline{/}\overline{\sum_{0}^{\ell=\infty}}(A_3 S_\ell + B_3 C_\ell) \overline{/} S_h C_k \qquad (8)$$

$$+ \underline{/}\overline{\sum_{0}^{\ell=\infty}}(A_4 C_\ell + B_4 S_\ell) \overline{/} S_h S_k \}$$

In this case, the summations over $\ell$ are carried out first. This results in a two-dimensional series with a constant value of z. If the results of the summations over $\ell$ are designated CC, CS, SC, and SS respectively, then equation (8) becomes

$$\rho(x,y,z) = \frac{2}{V} \sum_{0}^{h=\infty} \{ \underline{/}\overline{\sum_{0}^{k=\infty}}(CC \cdot C_k + (S \cdot S_k) \overline{/} C_h + \underline{/}\overline{\sum_{0}^{k=\infty}}(SC \cdot C_k +$$

$$SS \cdot S_k) \overline{/} S_h \} \qquad (9)$$

The final summation over h may be carried out assuming that the results of the k summations are designated COR and SIR, respectively.

$$\rho(x,y,z) = \frac{2}{V} \sum_{0}^{\infty}{}_{h} \mathrm{COR}\cdot C_h + \mathrm{SIR}\cdot S_h \qquad (10)$$

The program requires the information from a Friedel-unique hemisphere of data. However, for crystals with monoclinic or higher symmetry, the crystallographically unique data is less than a hemisphere. The remaining octants of data are generated within the program by applying space group symmetry.

Symmetry operation "a" operates on atoms at $\underline{r}_j$ according to the following

$$\underline{r}_j' = \underline{\underline{R}}_a \cdot \underline{r}_j + \underline{T}_a \ . \qquad (11)$$

Symmetry relations of this type enter the electron density expression through the exponential term, $\exp[-2\pi i\ \underline{h}^t \cdot (\underline{\underline{R}}_a \cdot \underline{r}_j + \underline{T}_a)]$. Rearranging this term generates a new reciprocal lattice vector, $\underline{h}^t{}_a$, such that

$$\underline{h}^t{}_a = \underline{h}^t \cdot \underline{\underline{R}}_a \qquad (12)$$

A consequence of the space group symmetry is that the magnitudes of the structure factors with the vectors $\underline{h}$ and $\underline{h}_a$ are equal.

Returning to the example described by equation (2), the vector $\underline{h}_a$ represents those vectors in the summation with negative h and/or k indices. Hence, equation (2) may be expressed as follows:

$$\rho(x,y,z) = \frac{M}{V} \sum_{1}^{N}_{n} \sum_{0}^{\infty}_{h} \sum_{0}^{\infty}_{k} \sum_{0}^{\infty}_{\ell} \{F(\underline{h}_n) \exp/\overline{-2\pi i \underline{h}^t_n} \cdot (\underline{r}+\underline{T}_n)/\overline{7} + F^*(-\underline{h}_n)\exp/\overline{-2\pi i(-\underline{h}^t_n)} \cdot (\underline{r}+\underline{T}_n)/\overline{7}\} \qquad (13)$$

in which the summation over n represents the inclusion of all (N) relevant symmetry operations. The factor M is a multiplicity term dependent upon the particular $\underline{h}$ and the Laué symmetry. Equation (13) becomes less formidable when it is realized that the term $\exp(-2\pi i \underline{h}^t_n \cdot \underline{T}_n)$ is really a phase shift applied to $F(\underline{h})$ to generate $F(\underline{h}_n)$. Defining the tangent of the phase of $F(\underline{h})$ as $B(\underline{h})/A(\underline{h})$, then the phase $\phi(\underline{h}_n)$ is related to $\phi(\underline{h})$ by

$$\phi(\underline{h}_n) = \phi(\underline{h}) - 2\pi \underline{h}^t \cdot \underline{T}_n \; . \qquad (14)$$

This type of phase shift is applied to all reflections internally generated by the program.

The orientation of the map is coordinated with the symmetry. A rotation matrix, corresponding to the chosen orientation, is multiplied into each of the rotation matrices. After this point in the program the h, k, and & indices are referred to as IR, IS, and IT corresponding to the across, down, and section summations, respectively. To save memory, the IR, IS, and IT integers are packed into one variable IRST.

## Program Details

A block diagram of the program is illustrated in Figure 11. Principal control is transferred from the main calling routine to four subroutines. Control information is written out in the subroutine STRT. Through the subroutine SETUPF, crystallographic data are input, and coefficients are determined and written to a temporary file. If necessary, the data are sorted by the subroutine QSORT. Finally the Fourier series calculations are carried out through the subroutine COMPF. A detailed description of the calculations is presented below.

The program begins by inputting control information and performing validity tests on the grid sizes and the output

Figure 11. A block diagram of the program FOUR.

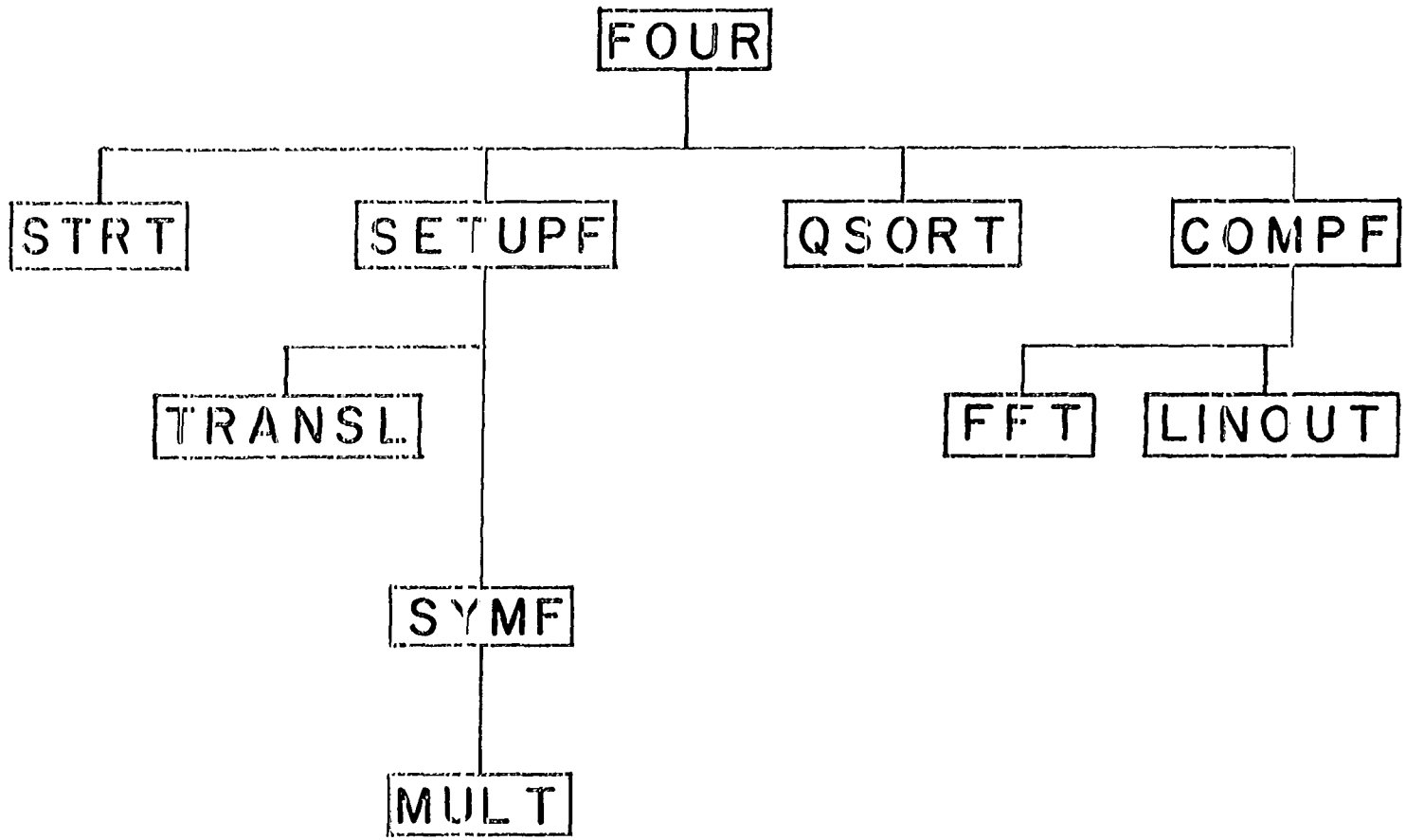
FOUR
STRT
SETUPF
QSORT
COMPF
TRANSL
FFT
LINOUT
SYMF
MULT

field width. These tests are included to terminate program execution before improper Fourier calculations might be made. Control is then transferred to STRT for the print out of control information and the determination of the orientation parameters. As described above, program control is then transferred to the routine SETUPF.

This routine begins by reading in symmetry information in a free format. The routine TRANSL then converts the character image symmetry information to rotation and translation matrices $\underline{\underline{R}}_n$ and $\underline{T}_n$. The symmetry matrices are printed out and then transformed according to the chosen orientation. A reflection with the hkl indices (000) is included in the data set, if requested. The reflection data is read in, one reflection at a time, and processed by the subroutine SYMF.

SYMF calculates and writes the appropriate $A_1$ through $A_4$ and $B_1$ through $B_4$ terms of equation (7) onto a temporary disk file. The A and B coefficients can, at present, represent any of seven different types of Patterson or electron density maps. The hkl values are packed into the variable IRST and written out with each data record. The multiplicity factor for each reflection is determined by the routine MULT. The number of data for each value of IR are calculated and stored in successive locations of the array IN.

After all reflection data are read in and processed, control is returned to the main calling routine. If automatic scaling is requested, the program computes a scale factor for which the origin peak is set to two times the largest number that can be printed with the given field width. The subroutine QSORT is then called if the data has not been presorted. (Data with orthorhombic or lower symmetry may be presorted first on the absolute value of the index corresponding to the summation down the page, then on the absolute value of the index in the across summation.)

The routine QSORT sorts the data based upon IRST according to the algorithm of R. C. Singleton (60). Because of array limits, the data are grouped in units of 700 or less based upon the IR index of each reflection. After each group is sorted, data with the same IRST are combined. All data in a given group are then written a temporary disk file. After all the data have been sorted, program control is transferred to the routine COMPF.

The Fourier series calculations are performed through the routine COMPF. Trigonometric factors are calculated at the beginning of the routine and stored in the arrays COSA, SINA, and S. The section and down summations are computed as described in equations (8) and (9), respectively.

The temporary results of the section summation are stored in the arrays CC, CS, SC, and SS. These arrays are dimensioned to hold up to 700 values, a practical number for crystal structures of small molecules.

The final summation is carried out by the routine FFT. This routine is an adaptation of a one-dimensional fast Fourier transform routine (61). FFT is designed to operate on a complex variable array yielding a transformed complex array. However, since the resultant function of crystallographic Fourier maps is real, the array input into FFT is compressed, reducing the size of the transform by a factor of two (62). Because of the modulo character of the fast Fourier transform, data with an IR index greater than or equal to half of the across grid size are not included in the summation.

After each line is calculated and scaled it is written to the appropriate output unit(s). As described above, data written to disk are written in integer representation. If printer output is requested, the routine LINOUT is called. This routine converts the output array to the appropriate number or character value and accumulates these values in a character array. When the entire line has been converted and stored, it is printed. Grid points which have values less than the user specified minimum are replaced with

blanks, and those grid points with values greater than the maximum allowed by the field width are replaced with asterisks.

## Conclusions

The program FOUR offers a versatile yet simple means for performing two- and three-dimensional Fourier series calculations. The program can be used with any space group symmetry. The program permits a wide range of map types and output modes.